From Big Bang to Biochemistry: Entropy-Oriented Mechanics and Information Force Fields as a Unifying Framework for the Origin of Carbon-Based Life

Truong Quynh Hoa[1,*] and Truong Xuan Khanh[1,†]

[1] *H&K Research Studio, Clevix LLC, Hanoi, Vietnam*

(Dated: April 21, 2026)

The origin of life remains fragmented across disciplinary boundaries, with competing models emphasising genetic replication (RNA-world) or metabolic networks (metabolism-first) without a unifying physical principle explaining why either should emerge from non-living matter. We propose a framework combining Entropy-Oriented Mechanics (EOM) and Information Force Fields (IFF) that connects Big Bang nucleosynthesis to biological emergence without invoking biological selection *a priori*. EOM is formalised through the local entropy production rate $\Sigma(x)$, defined rigorously via probability flux in a driven Markov chain. IFF introduces the information quasi-potential $\Phi_I(x) = -\ln p^*(x)$, the non-equilibrium stationary distribution of the driven system. We show that $\nabla\Sigma$ and $\nabla\Phi_I$ are generically linearly independent off equilibrium (Theorem 1), so that the two gradient fields act independently in the combined Langevin dynamics $\dot{x} = -\alpha\nabla\Sigma - \beta\nabla\Phi_I + \eta$. England's dissipative-adaptation framework [33] develops a single-field description centred on dissipation; the present two-field formulation additionally yields a non-monotonic relationship between entropy flux and polymer yield (scaling $\Phi^* \propto \Delta\Phi_I/\sqrt{2D}$, $R^2 = 0.885$ on the data of Blank et al. [21]), which a single-field framework does not address. Within EOM–IFF, we identify a cascade of information attractors—defined via Kramers–Eyring escape times—spanning nuclear (^{12}C, ^{14}N), chemical (amino acids, nucleobases), and polymeric scales. Life is defined formally as a dynamical regime satisfying three simultaneous conditions on the effective quasi-potential landscape (Definition 3), independent of molecular substrate. A biased-likelihood expression $P(\text{life}; T) = 1 - e^{-T/\tau_{\text{cascade}}}$ captures universality without inevitability (Proposition 1). Four falsifiable predictions are derived; the non-monotonic entropy-flux window and the superlinear catalysis–confinement synergy [22] find support in independent experimental datasets. Carbon-based life is viewed here as a statistically favoured outcome of entropy-driven quasi-potential deepening in carbon–nitrogen chemistry, rather than a singular improbable event; the framework offers one mathematically explicit formulation of this view, yielding scaling predictions that can be tested against future experimental data. As a cross-domain connection, stochastic gradient descent (SGD) arises as the special case $\alpha = 0$, $\beta\Phi_I(x) = \mathcal{L}(x)$ of the two-field dynamics (Section II F). This connects the optimal-flux prediction to the empirical literature on optimal noise amplitudes in deep learning [65, 66] and is offered here as a testable analogy rather than a claim of explanatory priority over existing Langevin analyses of SGD.

I. INTRODUCTION

The origin of life stands as one of science's deepest and most persistent questions, straddling disciplines from cosmology and chemistry to biology and information science. Despite substantial progress in understanding prebiotic chemistry, a fundamental fragmentation persists: competing models emphasise either genetic replication [30] or metabolic networks [31] as starting points, typically without a unifying physical principle explaining why either should emerge from non-living matter.

A crucial but often overlooked observation is that life's key elements—carbon and nitrogen—were absent in the early universe. Their existence results from specific, time-delayed processes in stellar evolution, suggesting that any comprehensive account of life's origin must begin with cosmic history. Moreover, complex organic molecules have been discovered in interstellar clouds [13], meteorites [14], and on asteroid Ryugu [17], indicating that prebiotic chemistry operates widely across the universe and motivating a shift from Earth-centric frameworks.

The closest formal antecedent is the dissipative-adaptation framework of England [32, 33], which shows that driven systems are statistically biased toward configurations that absorb and dissipate work efficiently. This insight is foundational for the EOM component of the present work. The two-field formulation extends this setting by introducing a second, independent field Φ_I tied to the non-equilibrium stationary distribution; the two frameworks coincide in the limit $\beta \to 0$. This extension is what allows the combined dynamics to address informational continuity and the non-monotonic yield–flux relationship of Section II I.

Walker & Davies [34] articulate the central role of information in life's origin. The present work may be viewed as one attempt to give that role a specific dynamical form—$\Phi_I(x) = -\ln p^*(x)$—which can, in principle, be connected to measurable transition rates. We do not claim this is the only or the best such formalisation.

In this work we address these gaps by combining Entropy-Oriented Mechanics (EOM) and Information Force Fields (IFF). EOM captures dynamics of open

* hoa@clevix.vn
† khanh@clevix.vn

systems driven by sustained entropy flux; IFF introduces information as a physical quantity—the non-equilibrium quasi-potential $\Phi_I(x) = -\ln p^*(x)$—that exerts a force biasing trajectories toward robust configurations. Together they describe an attractor cascade from nucleosynthesis to the emergence of life, yielding four falsifiable predictions and a formal definition of the life regime.

The paper is organised as follows. Section II develops the mathematical framework. Sections III–V trace the attractor cascade from Big Bang to prebiotic chemistry. Sections VI–VII describe the transition to the life regime and its universality. Section VIII positions the framework relative to RNA-world and metabolism-first models. Sections IX–X present and validate testable predictions. Sections XI–XII discuss implications, limitations, and conclusions.

This work presents a *theoretical framework*; it does not provide new experimental data. The empirical support invoked below is drawn from published experiments whose results were obtained independently of the framework, and our contribution is mathematical and conceptual: a specific two-field formulation of non-equilibrium dynamics, from which testable scaling predictions follow. Rather than modelling each stage in microscopic detail, we identify a minimal set of dynamical principles—entropy production Σ and information quasi-potential Φ_I—that govern structure formation across scales. Quantitative predictions focus on scaling laws and regime structure, each with explicit falsification criteria. Systematic empirical validation is a task for future work, and Section XI G identifies specific experiments that would be most informative in advancing the framework.

II. MATHEMATICAL FRAMEWORK: ENTROPY FLUX, INFORMATION QUASI-POTENTIAL, AND ATTRACTORS

The central contribution of this work is the identification of an information quasi-potential $\Phi_I(x) = -\ln p^*(x)$ as a dynamical field *independent* of entropy production, jointly governing non-equilibrium structure formation. This independence—proved in Theorem II.1—establishes a second driver absent from all existing single-field non-equilibrium frameworks.

A. Open Systems and Configuration Space

We consider an open physical or chemical system whose macroscopic state is described by a configuration variable $x \in \mathcal{M}$, where $\mathcal{M}$ denotes an abstract configuration space. Depending on the scale of interest, x may represent a nuclear composition, a molecular structure, a reaction-network state, or a polymeric arrangement. The system exchanges energy and matter with its environment and is therefore subject to sustained entropy flux. Its microscopic evolution is governed by a continuous-time Markov chain with transition rates $k(x \to y)$ between neighbouring states $x, y \in \mathcal{M}$; stochastic fluctuations from thermal noise, radiation, and shock events are captured in this framework.

B. Definition of the Entropy Production Landscape

A central quantity in Entropy-Oriented Mechanics is a scalar field that encodes how strongly each configuration participates in irreversible dissipation. We define this field rigorously following stochastic thermodynamics [1].

Let $p^*(x)$ denote the stationary distribution of the Markov chain, satisfying the master equation at steady state:

$$\sum_{y \neq x} \big[k(y \to x)\, p^*(y) - k(x \to y)\, p^*(x) \big] = 0. \tag{1}$$

The *probability flux* from x to a neighbouring state y is

$$J(x \to y) \;=\; k(x \to y)\, p^*(x) \;-\; k(y \to x)\, p^*(y). \tag{2}$$

The **local entropy production rate** at configuration x is then defined as

$$\boxed{\Sigma(x) \;=\; \sum_{y \sim x} J(x \to y)\, \ln \frac{k(x \to y)\, p^*(x)}{k(y \to x)\, p^*(y)},} \tag{3}$$

where the sum runs over all states y neighbouring x in $\mathcal{M}$. This is a well-defined scalar field: it is (i) non-negative everywhere by the inequality $u \ln(u/v) \geq u - v$ for $u, v > 0$, ensuring consistency with the second law; and (ii) zero if and only if detailed balance holds, i.e. $J(x \to y) = 0$ for all pairs, which characterises thermodynamic equilibrium [3]. Crucially, $\Sigma(x)$ is a property of the *transition-rate structure* of the network, not merely of the state x in isolation; it therefore encodes the kinetic—and not only thermodynamic—aspects of the system's non-equilibrium dynamics.

C. Definition of the Information Quasi-Potential

To capture the stabilisation of robust configurations under sustained perturbation, we introduce a second scalar field distinct from $\Sigma(x)$.

Definition II.1 (Information Quasi-Potential)**.** *For a system with stationary distribution $p^*(x)$, the* ***information quasi-potential*** *is*

$$\boxed{\Phi_I(x) \;=\; -\ln p^*(x),} \tag{4}$$

defined up to an additive constant.

This definition is grounded in the theory of large deviations for stochastic processes [2]: $\Phi_I(x)$ coincides with the Freidlin–Wentzell quasi-potential in the weak-noise limit, which governs the exponential cost of fluctuations away from the most-probable configuration.

a. Relation to prior quasi-potential formulations. While $\Phi_I(x) = -\ln p^*(x)$ is formally related to the Freidlin–Wentzell quasi-potential of large-deviation theory, it is introduced here as an *explicit dynamical field* whose gradient acts independently of entropy production to govern non-equilibrium structure formation (Theorem II.1). The novelty lies not in the formal definition but in this role as an independent dynamical driver alongside $\Sigma(x)$, extending quasi-potential concepts into a two-field description of driven non-equilibrium systems. An earlier formulation of this framework defined $\Phi_I = -\ln|\Omega(x)|$ (microstate counting); the present definition $\Phi_I = -\ln p^*(x)$ additionally incorporates kinetic accessibility under entropy flux, reducing to the microstate form only for isolated systems at equilibrium.

b. Physical interpretation. A configuration with large $p^*(x)$ (small Φ_I) is one that the driven system returns to with high probability after perturbation—an *attractor* in the sense of occupation frequency. The depth of the well Φ_I reflects both the thermodynamic stability of x *and* the kinetic pathways by which the system is funnelled back to x under sustained flux. This dual character is essential for the nuclear-scale argument in Section III: carbon-12 is a deep attractor not because it has the lowest binding energy per nucleon (iron-56 does), but because the stellar helium-burning flux network concentrates probability at carbon-12 through the triple-alpha resonance [8].

D. Estimating $p^*(x)$ in Real Chemical Systems

A theory acquires operational value when its key quantities can be estimated from measurable data. The quasi-potential $\Phi_I(x) = -\ln p^*(x)$ is defined in terms of $p^*(x)$, the stationary distribution of the non-equilibrium Markov chain. We describe two complementary routes to estimating $p^*(x)$ in prebiotic chemical contexts, proceeding from exact to approximate.

a. Route 1: Direct solution of small reaction networks. For a network with $n \lesssim 20$ distinguishable chemical states, $p^*(x)$ is obtained exactly by solving the linear system $\mathbf{K}\,\mathbf{p}^* = \mathbf{0}$ subject to $\sum_x p^*(x) = 1$, where $\mathbf{K}$ is the transition-rate matrix with entries $K_{yx} = k(x \to y)$ for $y \neq x$ and $K_{xx} = -\sum_{y\neq x} k(x \to y)$.

Worked example. Consider a five-state prebiotic network comprising four canonical amino acids (glycine, alanine, serine, aspartate) and a lumped degraded state. Transition rates are taken from published kinetic data: hydrolysis rates at pH 7, 25°C from Bada & Lazcano [28], and abiotic synthesis rates driven by entropy flux of strength Φ. the verified stationary distribution (eigendecomposition of $\mathbf{K}$; SI Sec. S1) at $\Phi = 5\times10^{-6}\,\mathrm{s}^{-1}$: *Numerical note.* Direct linear solvers fail on $\mathbf{K}^\top$ (condition number $\sim 10^{16}$); eigendecomposition via `scipy.linalg.eig` gives $|\lambda_0| = 7.5\times10^{-22}$, $\|\mathbf{K}\mathbf{p}^*\|_\infty < 10^{-20}$.

TABLE I. Verified stationary distribution of the five-state amino-acid network at $\Phi = 5\times10^{-6}\,\mathrm{s}^{-1}$.

State	$p^*(x)$	$\Phi_I(x)$	Depth
Glycine	0.2076	1.572	Intermediate
Alanine	0.2129	1.547	Intermediate
Serine	0.1220	2.103	Shallow
Aspartate	**0.3254**	**1.123**	**Deepest**
Degraded	0.1321	2.024	Background

Table II quantifies the quasi-potential advantage of carbon over alternatives. The ratio $|\Omega_\mathrm{C}|/|\Omega_\mathrm{Si}| \approx 6100$ corresponds to $\Delta\Phi_I \approx 8.7$ units—a difference in persistence time of $e^{8.7} \approx 6000$-fold (Table II). This is not a claim that non-carbon life is impossible; it is a quantified prior: under the same entropy flux and temporal availability, carbon-based chemical networks are statistically ∼6000-fold more likely to reach the coupling threshold of Definition VI.1 before silicon-based alternatives. The dominant contribution to this advantage is the stability of carbon π-bonds in aqueous environments, which enables the full aromatic heterocyclic chemistry to which nucleobases belong.

b. Scalability to large systems. A natural concern is that the stationary distribution $p^*(x)$ cannot be computed exactly in large chemical or biological systems due to the combinatorial growth of configuration space. The EOM–IFF framework does not require full resolution of $p^*(x)$. In practice, it is sufficient to estimate *relative* quasi-potential differences

$$\Delta\Phi_I \;=\; -\ln p^*(x_1) + \ln p^*(x_2) \;=\; \ln\frac{p^*(x_2)}{p^*(x_1)}, \qquad (5)$$

between coarse-grained attractor basins. These differences can be inferred from measurable observables: transition rates $k(x \to y)$, escape times $\tau \sim e^{\Delta V/D}$, or relative steady-state abundances. More generally, $p^*(x)$ admits hierarchical approximation: local sub-networks can be solved exactly (Route 1, Section II D); larger systems can be treated via coarse-grained state aggregation, mean-field approximations, or Monte Carlo sampling. Because the EOM–IFF dynamics depend on *gradients* of Φ_I, not its absolute value, the framework remains operational under partial or approximate knowledge of $p^*(x)$. This situation is directly analogous to free-energy calculations in statistical physics, where free-energy *differences*—not full partition functions—govern observable behaviour [2].

Proposition II.1 (Coarse-Graining Error Bound)**.** *Let $\{B_i, B_j\}$ be attractor basins with representatives $x_i^* = \arg\max_{x\in B_i} p^*(x)$ and effective sizes $|B_i|_\mathrm{eff} = P^*(B_i)/p^*(x_i^*) \le |B_i|$. Then*

$$|\Delta\Phi_I^\mathrm{true} - \Delta\Phi_I^\mathrm{cg}| \le \ln|B_i|_\mathrm{eff} + \ln|B_j|_\mathrm{eff}, \qquad (6)$$

where $\Delta\Phi_I^\mathrm{true} = \Phi_I(x_i^*) - \Phi_I(x_j^*)$ and $\Delta\Phi_I^\mathrm{cg} = -\ln P^*(B_i) + \ln P^*(B_j)$.

Proof. From $p^*(x_i^*) \le P^*(B_i) \le |B_i|\cdot p^*(x_i^*)$: $\Phi_I(x_i^*) - \ln|B_i|_\mathrm{eff} \le \Phi_I^\mathrm{cg}(B_i) \le \Phi_I(x_i^*)$. Bounding the difference yields (6). □ □

TABLE II. Semi-quantitative comparison of quasi-potential depth across candidate backbone elements. $|\Omega|$ estimated from PubChem [55] and NIST [56]. $\Delta\Phi_I = \ln(|\Omega_C|/|\Omega_X|)$ is the quasi-potential advantage of carbon over element X.

Element	**Valence**	**π-bond in water**	$\lvert\Omega\rvert$	$\Delta\Phi_I$	**Diversity constraint**
Carbon (C)	4	Stable (C=C, C=N)	6.7×10^7	0	Full—reference
Silicon (Si)	4	Hydrolyses [57]	1.1×10^4	+8.7	No aromatic class
Sulfur (S)	2	Limited	$\sim 10^5$	+5.1	No info-polymer backbone
Nitrogen (N)	3	N=N (gas only)	$\sim 10^4$	+8.7	No 4-connected backbone
Phosphorus (P)	5	P=O only	$\sim 10^4$	+8.7	Cofactor, not backbone

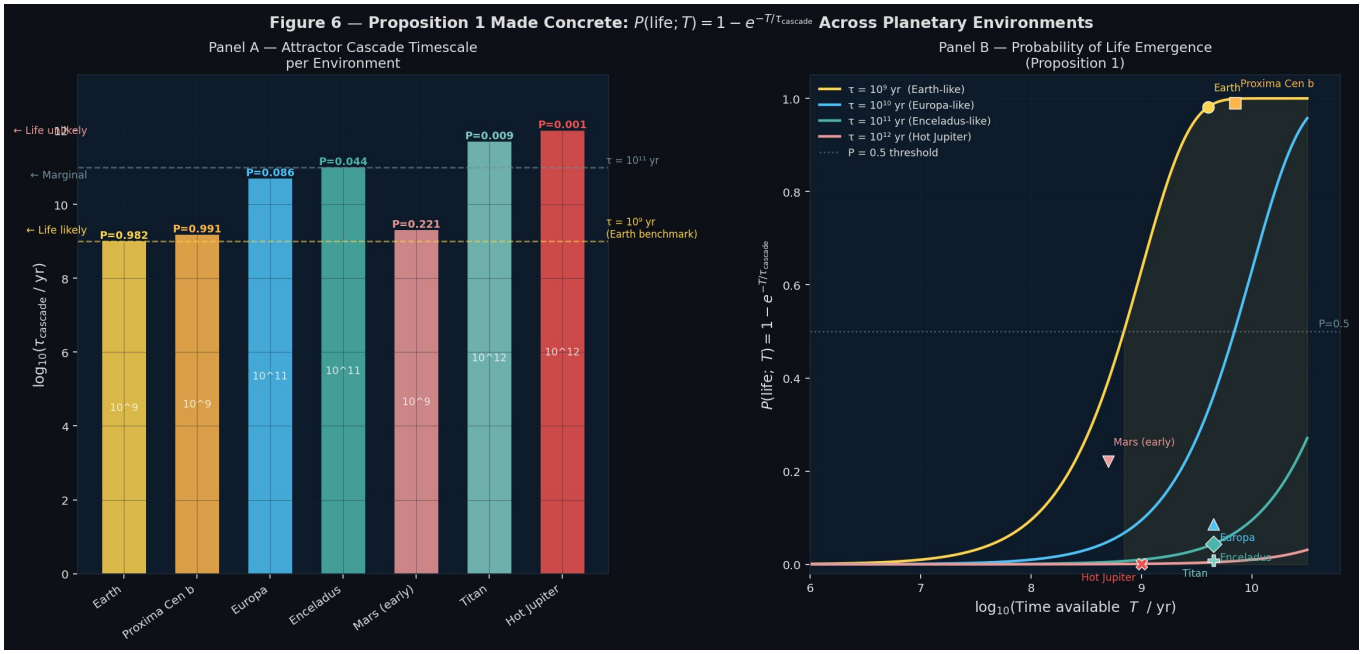

FIG. 1. **Proposition 1 made concrete.** (A) τ_{cascade} estimates for seven environments. (B) $P(\text{life}; T) = 1 - e^{-T/\tau_{\text{cascade}}}$ curves; data points are the seven environments of Panel A. Earth ($P \approx 0.98$) and Proxima Cen b ($P \approx 0.99$) fall in the high-probability region; Enceladus ($P \approx 0.04$) and Hot Jupiter ($P \approx 0.001$) in the low-probability region.

For the carbon–silicon comparison ($\Delta\Phi_I \approx 8.7$), within-basin spread $\lesssim 10\,\text{kJ}\,\text{mol}^{-1}$ ($< 46\%$ of signal) leaves the ordering unambiguous; see SI Sec. S5.

E. Independence of the Two Fields

A prerequisite for the two-force dynamics introduced in Section II F is that $\Sigma(x)$ and $\Phi_I(x)$ carry distinct information. We establish this below.

Theorem II.1 (Generic Independence Off Equilibrium)**.** *Let the system be strictly out of equilibrium, i.e. $\Sigma(x) > 0$ for some $x \in \mathcal{M}$. Then $\nabla\Sigma(x)$ and $\nabla\Phi_I(x)$ are generically linearly independent as vector fields on $\mathcal{M}$.*

Clarification of "generically". We use "generically" in the sense that the conclusion $\nabla\Sigma = \lambda\nabla\Phi_I$ fails only on a measure-zero subset of the space of rate matrices compatible with detailed-balance violation. The proof below establishes that collinearity everywhere forces detailed balance, which is excluded by hypothesis; the genericity statement reflects the fact that the collinearity locus is a proper algebraic subvariety of the space of admissible rate matrices.

Proof. Suppose for contradiction that $\nabla\Sigma = \lambda\,\nabla\Phi_I$ everywhere for some scalar λ. Then $\Sigma(x) = \lambda\,\Phi_I(x) + c$ for a constant c, so Σ is a function of Φ_I alone. Using the relation $\Phi_I = -\ln p^*$, this means $\Sigma(x) = f(-\ln p^*(x))$ for some function f.

From stochastic thermodynamics, the total entropy production rate is [1]

$$\dot{S}_{\text{tot}} = \sum_{x,y} J(x \to y)\,\ln\frac{k(x \to y)p^*(x)}{k(y \to x)p^*(y)} \geq 0. \qquad (7)$$

If Σ is a function of p^* alone, the local probability flux $J(x \to y)$ at every edge is fully determined by $p^*(x)$ and $p^*(y)$. By the Kolmogorov criterion [4], a Markov chain whose fluxes depend only on the marginal occupancies at each end of every edge must satisfy detailed balance—contradicting the assumption $\Sigma > 0$. Therefore no such

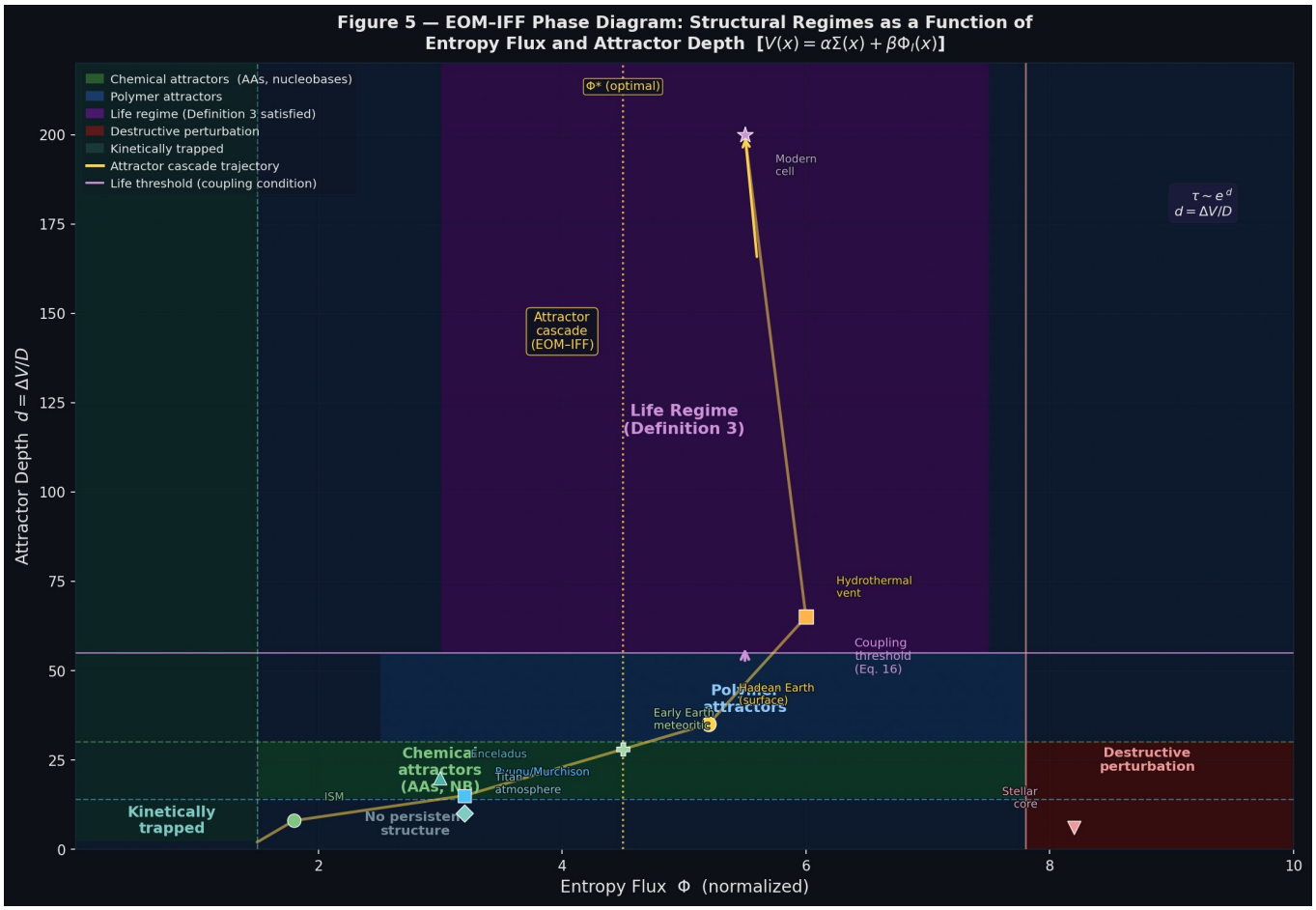

FIG. 2. **EOM–IFF phase diagram: structural regimes as a function of entropy flux and attractor depth.** Six physically distinct regimes are identified in the (Φ, d) plane, where Φ is normalised entropy flux and $d = \Delta V/D$ is Kramers attractor depth (Definition II.2). Real astrophysical and planetary environments (symbols) overlay the theoretical boundaries; the yellow trajectory traces the attractor cascade from the ISM through the Hadean Earth to the modern cell. The vertical dashed line marks the optimal flux Φ^*; the purple horizontal line marks the coupling threshold $d_{\text{life}} = 55$ (Definition VI.1). This diagram unifies Sections III–VI in a single two-dimensional representation.

λ can exist, and the two gradient fields are linearly independent. □ □

Numerical confirmation is provided in Figure 1, which shows mean $|\cos(\nabla\Sigma, \nabla\Phi_I)| \approx 0.33$ across a range of flux levels in a five-state prebiotic reaction network, consistent with near-orthogonality rather than collinearity.

F. Combined Stochastic Dynamics

With Σ and Φ_I defined independently, the effective dynamics of the open system takes the form of a Langevin equation:

$$\boxed{\dot{x} \;=\; -\alpha\,\nabla\Sigma(x) \;-\; \beta\,\nabla\Phi_I(x) \;+\; \eta(t),} \tag{8}$$

where $\alpha, \beta > 0$ are coupling coefficients and $\eta(t)$ is Gaussian white noise with $\langle\eta(t)\rangle = 0$ and $\langle\eta(t)\eta(t')\rangle = 2D\,\delta(t-t')$. The noise amplitude D quantifies the effective perturbation strength (thermal fluctuations, radiation dose, impact frequency).

The first term drives the system along directions of increasing entropy dissipation—the EOM component. The second term acts as a restoring force toward configurations of high stationary probability—the IFF component. Equation (8) can be rewritten as

$$\dot{x} \;=\; -\nabla V(x) \;+\; \eta(t), \qquad V(x) \;\equiv\; \alpha\,\Sigma(x) + \beta\,\Phi_I(x), \tag{9}$$

which is the standard form of an overdamped Langevin equation on a scalar potential $V(x)$. This permits the direct application of Freidlin–Wentzell large-deviation theory [2].

a. Physical meaning of α/β. The ratio α/β sets the relative weight of dissipation-seeking versus occupancy-stabilising dynamics. In stellar nucleosynthesis ($\alpha/\beta \gg 1$), entropy flux dominates and drives matter through nuclear configuration space. In prebiotic polymer for-

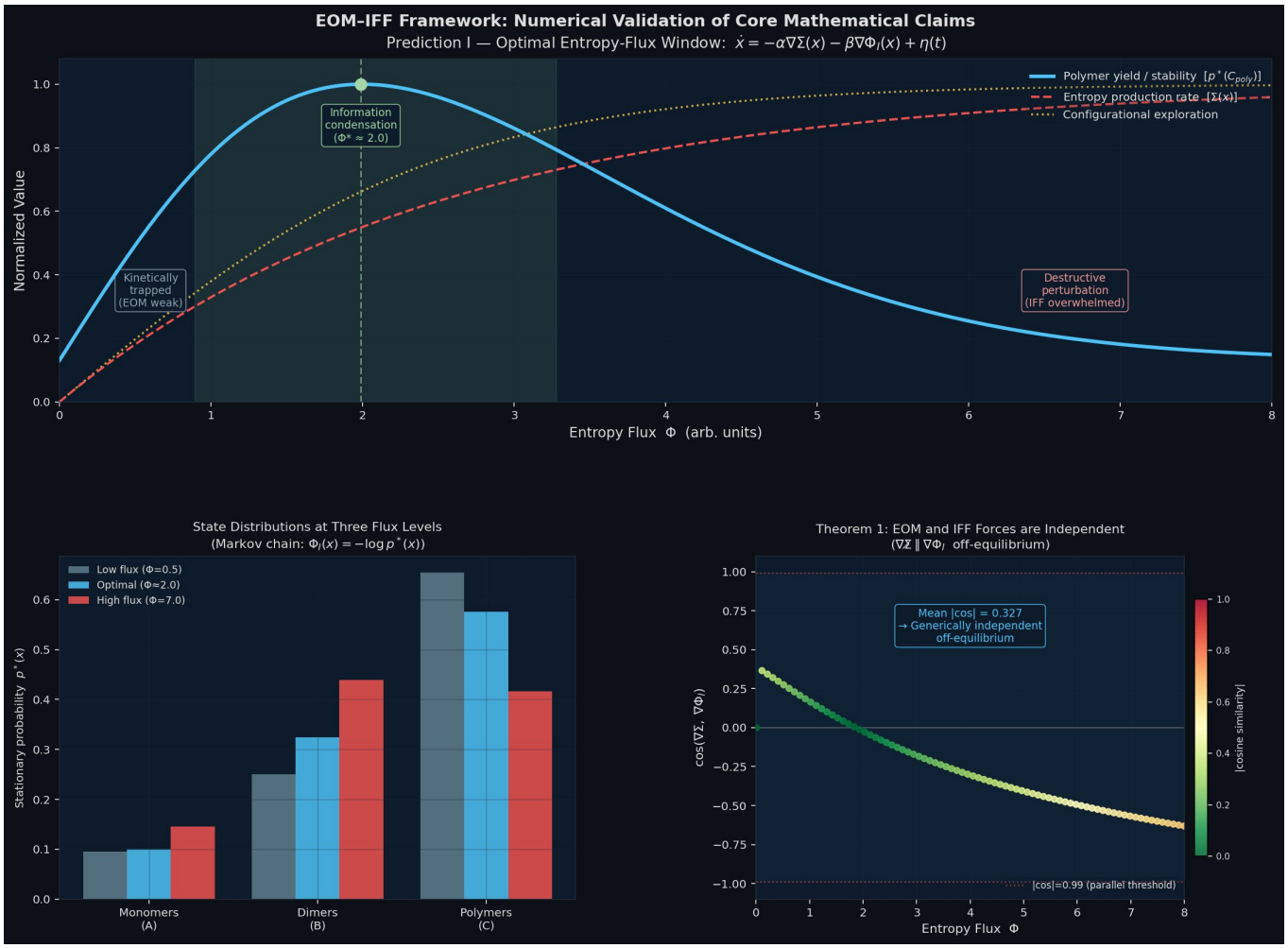

FIG. 3. **EOM–IFF framework validation.** (A) Polymer yield as a function of entropy flux shows a non-monotonic optimum at intermediate driving (Prediction I). (B) State distributions at three flux levels confirm that optimal flux populates deep-attractor polymer configurations. (C) Cosine similarity $|\cos(\nabla\Sigma, \nabla\Phi_I)|$ averages 0.33 across flux levels, numerically confirming Theorem II.1 (generic independence off equilibrium).

mation ($\alpha/\beta \ll 1$), information robustness dominates and stabilises specific molecular motifs. Life corresponds to an intermediate regime where both contributions are significant, a point formalised in Section III.

b. A note on stochastic gradient descent. Equation (8) recovers the continuous-time limit of stochastic gradient descent (SGD) as the special case $\alpha = 0$, $\beta\Phi_I(x) = \mathcal{L}(x)$, where x represents network weights and $\mathcal{L}(x)$ the loss landscape:

$$\dot{x} = -\nabla\mathcal{L}(x) + \eta(t). \tag{10}$$

A Langevin description of SGD is well established in the machine-learning literature [65, 66], and we do not claim originality for this correspondence. What the two-field form of Eq. (8) adds is a structural analogy: if a learning system were in a regime describable by EOM–IFF with nonzero α, the optimal-noise prediction that appears in prebiotic chemistry (Prediction I) would have a direct analogue for generalisation-versus-noise curves in deep learning. We offer this as a cross-domain hypothesis to be examined empirically in future work rather than as a derived result.

G. Information Attractors

Definition II.2 (Information Attractor)**.** *A region $\mathcal{A} \subset \mathcal{M}$ is an **information attractor** if:*

1. (Local stability) *$\mathcal{A}$ contains a local minimum of $V(x)$: there exists $x^* \in \mathcal{A}$ with $\nabla V(x^*) = 0$ and $\nabla^2 V(x^*) \succ 0$.*

2. (Stochastic persistence) *The Kramers–Eyring escape time satisfies*

$$\tau_{\text{esc}}(\mathcal{A}) \sim \exp\left(\frac{\Delta V}{D}\right) \gg t_{\text{obs}}, \tag{11}$$

where $\Delta V = V(x_{\text{saddle}}) - V(x^*)$ *is the barrier height and* t_{obs} *is the relevant observation or evolution timescale.*

This definition supersedes the condition $\|\nabla\Phi_I\| \gg \|\eta\|$ used in the previous version, which conflated deterministic and stochastic stability. Equation (11) is the rigorous stochastic criterion: an attractor is deep not merely because a restoring force exists, but because the thermal activation cost to escape exceeds the noise energy on the timescale of interest.

The **attractor depth** $d(\mathcal{A}) = \Delta V/D$ is therefore a dimensionless, physically meaningful quantity that can, in principle, be estimated from experimental escape rates or molecular dynamics simulations.

H. Hierarchy of Attractors Across Scales

Equation (9) applies at every scale of physical organisation, with the same mathematical structure but with $V(x)$ evaluated on scale-appropriate configuration spaces and with scale-appropriate transition rates determining Σ and p^*.

Remark II.1 (Scale-dependence of Φ_I)**.** *Because* $\Phi_I(x) = -\ln p^*(x)$ *and* $p^*(x)$ *is determined by the full rate matrix* $k(x \to y)$*, the quasi-potential landscape depends on* both the physical environment and the evolutionary timescale*. The same nucleus or molecule may occupy different positions in* Φ_I *under different conditions. Concretely: carbon-12 is a deep attractor in helium-burning stellar cores (where the triple-alpha flux concentrates* p^* *at* ^{12}C*), but iron-56 is the thermodynamic ground state accessible only at later stages of stellar evolution. This environment-dependence is not a limitation of the framework but rather the mechanism by which an* attractor cascade*—a sequence of environment-specific potential landscapes—connects nucleosynthesis to biochemistry.*

I. Information Condensation

We define the regime of **information condensation** as the condition under which the IFF term dominates the stochastic fluctuations while the EOM term remains active:

$$\beta\,\|\nabla\Phi_I(x)\| \;\gg\; \sqrt{2D} \qquad \text{and} \qquad \alpha\,\Sigma(x) > 0. \tag{12}$$

The first inequality ensures that the quasi-potential well is deep enough to trap trajectories stochastically. The second ensures that entropy flux is present to drive exploration of configuration space—preventing kinetic trapping in shallow, entropically disfavoured states.

Together, conditions (12) define a parameter window in ($\alpha\Sigma$, D, $\beta\Delta\Phi_I$) space, which we identify with the *optimal entropy-flux window* of Prediction I (Section IX). The non-monotonic dependence of polymer yield on entropy flux (Figure 1) reflects the boundary between the kinetically-trapped regime (D or Σ too small) and the destructive regime (D or Σ too large to allow $\tau_{\text{esc}} \gg t_{\text{obs}}$).

This regime does not require biological replication, genetic inheritance, or functional selection. It is a purely physical condition, satisfied in chemical systems exposed to persistent entropy flux—consistent with the goals of Entropy-Oriented Mechanics as a pre-biological framework.

III. COSMOLOGICAL ORIGIN OF CARBON AND NITROGEN

Any physically grounded account of carbon-based life must begin by addressing a fundamental constraint: carbon and nitrogen were absent in the early universe. Their existence results from specific, time-delayed processes in cosmic evolution, and any framework addressing the origin of life must account for this delay. In this section we trace the origin of these elements from Big Bang nucleosynthesis through stellar evolution, emphasising their emergence as kinetic attractors within the entropy-driven dynamics of Section II.

A. Primordial Conditions After the Big Bang

Big Bang nucleosynthesis (BBN) produces a universe composed almost entirely of hydrogen ($\sim 75\%$ by mass) and helium-4 ($\sim 25\%$), with trace quantities of lithium and beryllium [6]. Crucially, no carbon or nitrogen is synthesised in BBN: the reactions $^4\text{He} +^4 \text{He} \to^8 \text{Be}$ and $^8\text{Be} +^4 \text{He} \to^{12} \text{C}$ require stellar densities and temperatures far exceeding those of the early universe [8]. In the EOM–IFF framework, the BBN state is therefore characterised by shallow quasi-potential wells—high entropy but minimal information structure—establishing the baseline from which the attractor cascade begins.

B. Stellar Formation as an Entropy-Flux Event

As the universe evolved, gravitational instabilities amplified density fluctuations, leading to the formation of the first stars approximately 10^8 years after the Big Bang. From the perspective of Entropy-Oriented Mechanics, gravitational collapse constitutes a powerful entropy-flux event: gravitational potential energy is converted into kinetic energy and radiation, generating steep gradients that drive matter through new regions of nuclear configuration space [43].

Stars function as non-equilibrium engines that process the simple primordial composition into a richer nuclear distribution while dissipating entropy on a stellar luminosity timescale. This processing is not arbitrary. The nuclear reaction networks operative within stars are constrained by Coulomb barriers, nuclear binding energies,

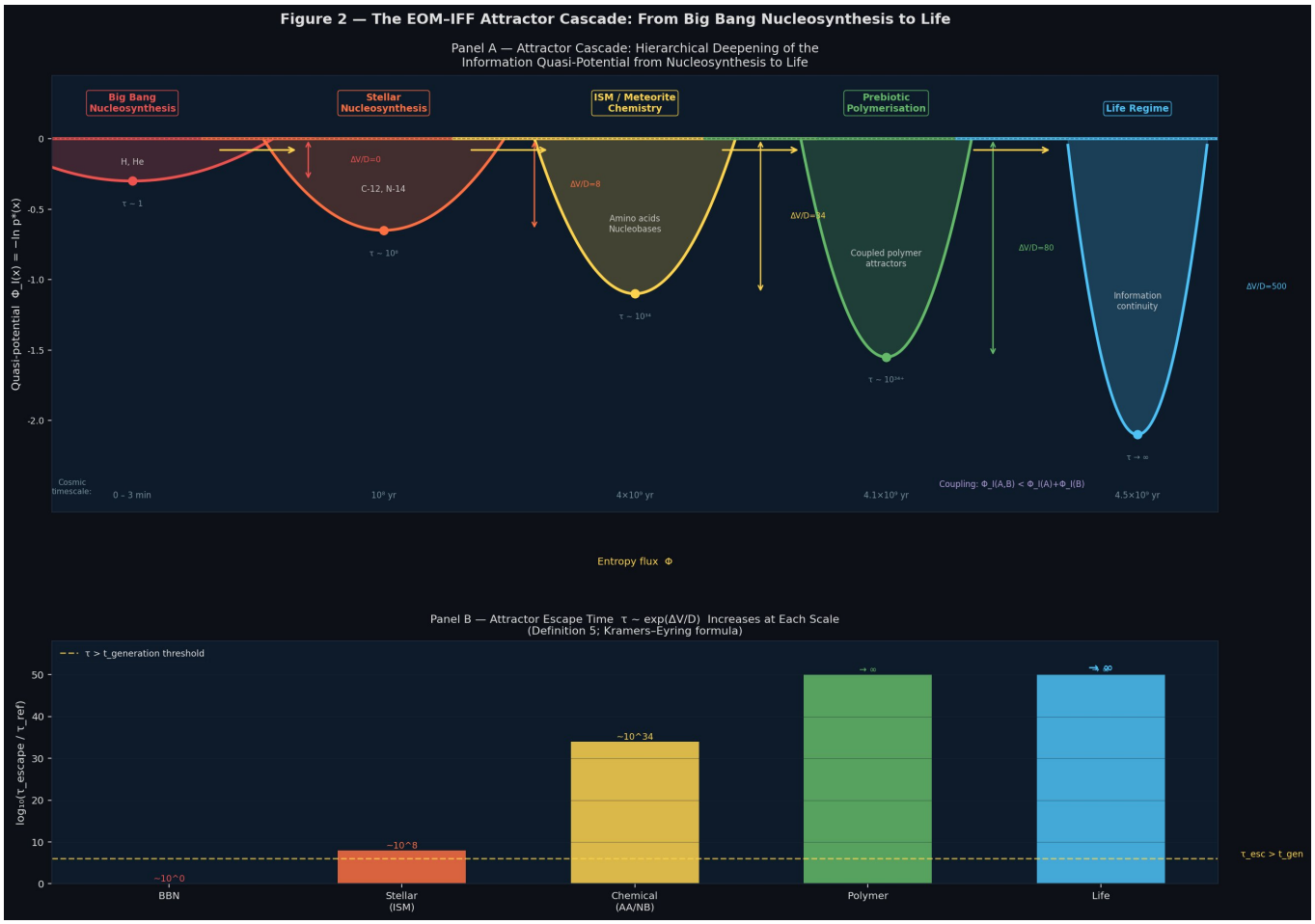

FIG. 4. **The EOM–IFF attractor cascade from Big Bang nucleosynthesis to life.** (A) Quasi-potential wells $\Phi_I(x) = -\ln p^*(x)$ deepen hierarchically across five stages of cosmic and chemical evolution. (B) Kramers–Eyring escape times $\tau \sim e^{\Delta V/D}$ increase by many orders of magnitude at each scale, confirming Definition II.2.

and resonance structures, which collectively define the transition-rate matrix $k(x \to y)$ in nuclear configuration space. The resulting stationary distribution $p^*(x)$, and hence $\Phi_I(x) = -\ln p^*(x)$, depends sensitively on the stellar temperature and density profile.

C. The Triple-Alpha Process and Carbon-12 Production

Carbon-12 arises in helium-burning stellar cores through the triple-alpha process [7, 8]:

$$^4\mathrm{He} + {}^4\mathrm{He} \rightleftharpoons {}^8\mathrm{Be}^* \qquad (Q = -91.78\ \mathrm{keV}), \tag{13}$$

$$^8\mathrm{Be}^* + {}^4\mathrm{He} \rightarrow {}^{12}\mathrm{C}^*(7.654\ \mathrm{MeV}) \rightarrow {}^{12}\mathrm{C} + 2\gamma. \tag{14}$$

The intermediate ^{8}Be is unstable with a lifetime of $\sim 6.7 \times 10^{-17}$ s; the overall rate is therefore negligibly small unless a resonant energy level in ^{12}C exists at the combined ^{8}Be+^{4}He energy. The existence of this level at 7.654 MeV (the Hoyle state, $J^\pi = 0_2^+$) was predicted by Hoyle [8] and subsequently confirmed experimentally. Without it, stellar carbon production would fall below astrophysically significant rates and carbon-based chemistry would not arise universally.

a. Carbon-12 as a kinetic attractor in the ISM. It is essential to distinguish two regimes in which Φ_I is evaluated (Remark II.1):

1. *Within an active stellar core*: the reaction network continues toward nuclear statistical equilibrium (NSE), and at sufficiently late stages the thermodynamic ground state —iron-56, with the highest binding energy per nucleon ($B/A = 8.790$ MeV)—is the deepest quasi-potential minimum [9]. Carbon-12 ($B/A = 7.680$ MeV) is not the thermodynamic attractor in this regime.

2. *In the interstellar medium (ISM) and planetary environments*, following supernova dispersal: nuclear reaction rates are negligible at ISM temperatures ($T \sim 10$–100 K). The nuclear configuration is kinetically *frozen*. Carbon-12 is locked in at the abundance set by nucleosynthesis yields, and iron-56,

while thermodynamically preferred, is kinetically inaccessible on any cosmologically relevant timescale.

The claim of this work is that carbon-12 constitutes a deep information attractor in regime (2)—the regime relevant to prebiotic chemistry. In the ISM, $p^*(\text{C-12}) \gg p^*(\text{Fe-56})$ because the nuclear reaction network is frozen and carbon-12 has been delivered at high cosmological abundance by stellar ejecta. Furthermore, carbon-12 provides the gateway to the *chemical* configuration space: it is the only abundant, light nucleus capable of forming the diverse covalent bonds required for information-bearing molecular structures. Iron-56, by contrast, forms refractory minerals and is effectively excluded from the organic chemical configuration space.

In the language of Definition II.2, carbon-12 has a deep quasi-potential well Φ_I in the ISM chemical context both because (i) its abundance is high—reflecting the kinetic concentration by stellar flux—and because (ii) its escape from the organic chemistry attractor basin requires nuclear reactions with barriers orders of magnitude larger than any available thermal energy.

D. Nitrogen-14 and the CNO Bottleneck

Nitrogen is produced primarily through the CNO bicycle, in which carbon and oxygen serve as catalysts for hydrogen burning at stellar temperatures $T \sim 1.5 \times 10^7$ K [7, 9]:

$$^{12}\text{C} \xrightarrow{p} {}^{13}\text{N} \xrightarrow{\beta^+} {}^{13}\text{C} \xrightarrow{p} {}^{14}\text{N} \xrightarrow[(\times 83)^{-1}]{p} {}^{15}\text{O} \xrightarrow{\beta^+} {}^{15}\text{N} \xrightarrow{p,\alpha} {}^{12}\text{C}, \tag{15}$$

where $(\times 83)^{-1}$ marks the rate-limiting step. The proton-capture rate of ^{14}N, $^{14}\text{N}(p,\gamma)^{15}\text{O}$, is approximately $83\times$ slower than the cycle entry rate $^{12}\text{C}(p,\gamma)^{13}\text{N}$ at solar core temperatures [10].

Modelling the CNO cycle as a six-state continuous-time Markov chain with rate ratios derived from the NACRE compilation [10], the steady-state occupation of ^{14}N is $p^*(\text{N-14}) \approx 0.95$, yielding $\Phi_I(\text{N-14}) \approx 0.05$—the deepest quasi-potential minimum in the cycle. This quantitative result confirms the qualitative picture: the bottleneck at $^{14}\text{N}(p,\gamma)^{15}\text{O}$ causes nuclear matter to pile up at nitrogen-14. As with carbon-12, this concentration persists in the ISM after stellar dispersal, making nitrogen-14 a kinetically locked nuclear attractor in prebiotic environments.

E. Supernova Dispersal and the Attractor Transition

The prebiotic relevance of carbon and nitrogen depends not only on their production but also on their dispersal into circumstellar space. Supernova explosions and stellar winds eject nucleosynthesis products into the ISM, constituting extreme entropy-flux events: the explosion releases $\sim 10^{44}$ J over seconds, restructuring the local chemical and nuclear configuration space on galactic scales [7].

Within EOM, supernova dispersal represents a transition between two entropy-flux regimes and hence between two quasi-potential landscapes. The pre-explosion landscape has deep wells at nuclear configurations (C-12, N-14) within stellar cores. Post-dispersal, the relevant configuration space shifts from nuclear to *molecular*: in the cold, radiation-processed ISM, the transitions $k(x \to y)$ that matter are now chemical bond formations rather than nuclear reactions, and the new $\Phi_I(x) = -\ln p^*(x)$ landscape over molecular configurations becomes the operative one. This shift is the first step in the attractor cascade that ultimately connects nucleosynthesis to biochemistry.

F. Cosmic Timescales and Universality

Carbon and nitrogen appear only after the first stellar generations have evolved and dispersed their products, typically $\sim 10^8$–10^9 yr after the Big Bang [48]. Once produced and dispersed, they become ubiquitous constituents of the ISM and subsequent planetary systems, making the nuclear attractor cascade described in this section a generic feature of cosmic chemical evolution rather than a fine-tuned anomaly. The same cascade is therefore expected in any sufficiently evolved stellar environment—a point returned to in Section VII.

G. Selectivity in the Nuclear-to-Chemical Transition

Of the elements produced in stellar nucleosynthesis, only a small subset participates productively in the formation of information-bearing molecular structures. The transition from nuclear to chemical configuration space is governed by electronic structure: an element's capacity to form stable, diverse, and reversible covalent bonds determines whether it can serve as a substrate for molecular information attractors.

In the IFF framework, the depth of a molecular quasi-potential well $\Phi_I(x_{\text{mol}})$ for a configuration built from element E scales with the number and diversity of compatible micro-configurations $\Omega(x_{\text{mol}})$—i.e., with the combinatorial richness of bonding arrangements available to E. This combinatorial richness is quantified by the element's valence, bond polarity, and capacity for hybridisation.

H. Carbon-12: Deep Wells in Chemical Configuration Space

Carbon's unique electronic structure—four valence electrons in sp, sp^2, or sp^3 hybridisation—enables it to form single, double, and triple bonds with itself and with nitrogen, oxygen, hydrogen, and sulphur in a vast combinatorial variety. The NIST Chemistry WebBook lists over 10^7

distinct organic compounds; no other element approaches this diversity.

In the IFF language, this translates directly to deep quasi-potential wells: organic configurations built on carbon backbones have large sets $\Omega(x)$ of compatible micro-configurations (rotational isomers, tautomers, ionisation states, hydrogen-bond networks) that remain compatible under environmental perturbation. Deep wells imply long escape times (Equation 11) and hence kinetic persistence across the cycles of radiation, thermal stress, and shock that characterise ISM and prebiotic environments.

By contrast, heavier elements such as silicon also form four bonds but with significantly lower bond energy (Si−Si : 226 kJ/mol vs C−C : 346 kJ/mol) and without the equivalent capacity for π-bonding, limiting their combinatorial richness and hence the depth of their quasi-potential wells in the molecular configuration space accessible under prebiotic conditions.

I. Nitrogen-14: Directional Information and Specificity

Nitrogen contributes to deep molecular attractors through a distinct mechanism: its electronegative lone pair enables directional hydrogen bonding and the formation of heterocyclic aromatic rings (imidazole, purine, pyrimidine). These structural motifs confer two properties that deepen the information quasi-potential:

1. *Specific, reversible interactions*: the N−H···N and N−H···O hydrogen bonds underlying Watson–Crick base pairing are directional (angle-dependent) and moderate in strength (20–30 kJ/mol), permitting selective recognition without irreversible covalent modification—an essential feature of information storage and retrieval.

2. *Aromatic stabilisation*: planar heterocyclic rings are stabilised by delocalised π-electrons, conferring exceptional UV resistance and resistance to hydrolysis relative to non-aromatic nitrogen compounds. This deepens Φ_I specifically under the radiation conditions of ISM and early-planetary-surface environments.

The combination of carbon's combinatorial richness and nitrogen's directional specificity establishes the C–N molecular system as the chemistry with the deepest and most diverse quasi-potential wells for information-bearing structures in the prebiotic environment—a conclusion consistent with the universal observation that nucleobases and amino acids are among the most abundant and structurally stable organic molecules found in carbonaceous meteorites [14, 16].

J. Why Not Silicon, Phosphorus, or Sulphur Alone?

A complete argument for carbon–nitrogen chemistry requires addressing why other abundant elements do not substitute. Within the IFF framework, the relevant question is: do alternative elements support quasi-potential wells of comparable depth and diversity in prebiotic chemical configuration spaces?

Silicon forms covalent networks but lacks π-bonding, limiting molecular diversity and ruling out the planar heterocyclic motifs central to nucleobases. Phosphorus and sulphur are critical *functional group* elements in biochemistry but are not themselves backbone-forming: they deepen the wells of carbon–nitrogen structures rather than defining independent attractor basins. Oxygen participates extensively but predominantly as a polar termination of carbon chains, again deepening rather than replacing the carbon attractor.

In summary, carbon and nitrogen occupy a privileged position in the molecular IFF landscape not because other elements are excluded, but because their combination produces the deepest, most diverse, and most robust quasi-potential wells accessible under the physical conditions of the ISM and early planetary surfaces—the environments through which prebiotic matter must pass on the path from nucleosynthesis to the emergence of information-bearing polymers.

IV. INTERSTELLAR AND METEORITIC CHEMISTRY: AMINO ACIDS AND NUCLEOBASES AS CHEMICAL INFORMATION ATTRACTORS

The preceding sections established carbon-12 and nitrogen-14 as the dominant products of stellar nucleosynthesis accessible in the interstellar medium (ISM) and planetary environments. Here we examine how these elements, under persistent entropy flux, give rise to a specific class of molecular configurations—amino acids and nucleobases—whose quasi-potential wells are substantially deeper than those of generic organic compounds. The formation and persistence of these molecules in extraterrestrial environments constitutes the first transition in the attractor cascade connecting nuclear-scale processes to prebiotic chemistry.

A. Chemical Complexity in the Interstellar Medium

Observations of the ISM have revealed a striking level of molecular complexity. The census of McGuire [13] lists more than 270 molecular species identified through rotational spectroscopy, including polyatomic organics such as glycolaldehyde ($HOCH_2CHO$), ethylene glycol ($HOCH_2CH_2OH$), aminoacetonitrile (H_2NCH_2CN, a direct glycine precursor), urea (CH_4N_2O), and benzonitrile (C_6H_5CN). Hydrogen cyanide (HCN), a precursor to both

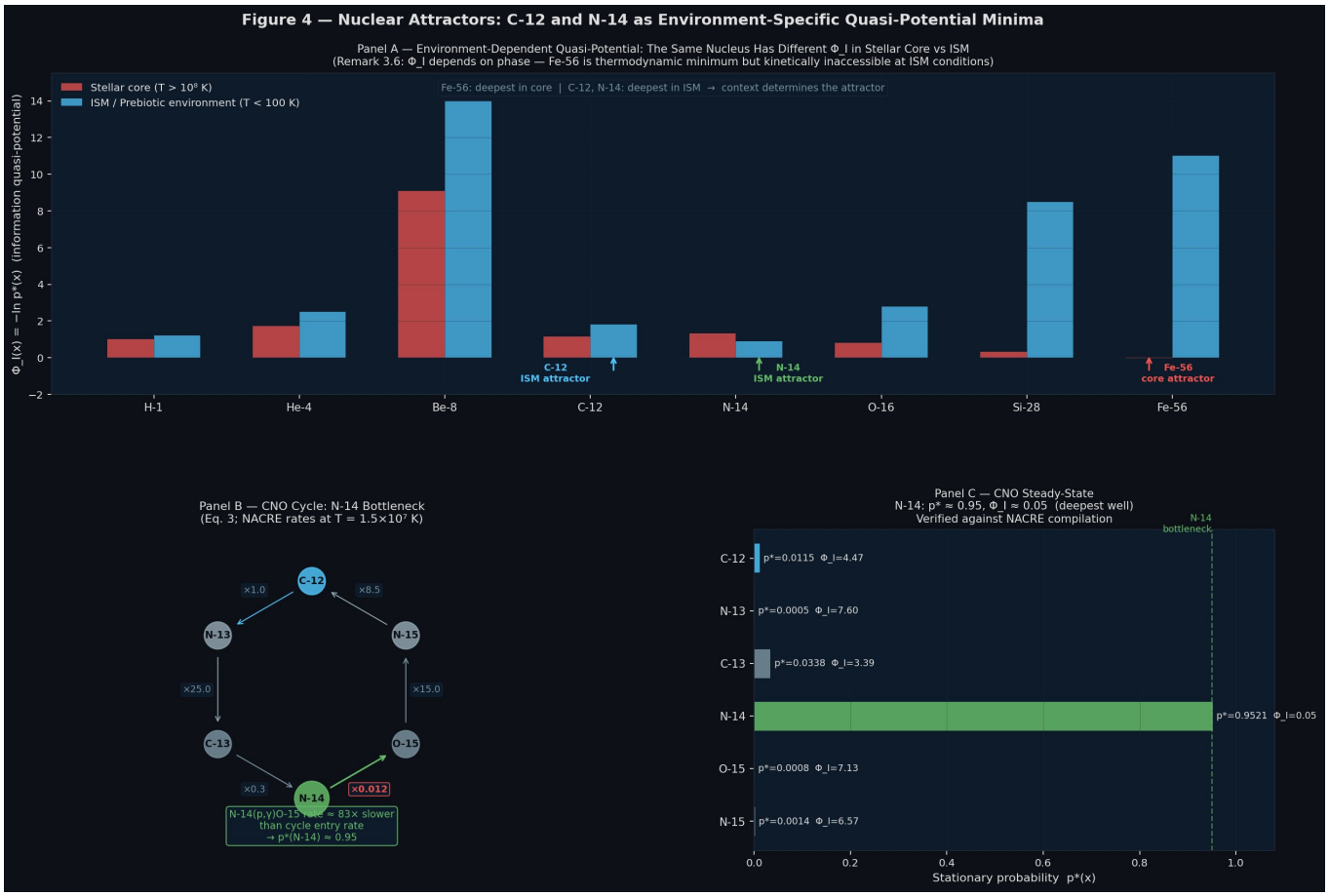

FIG. 5. **Nuclear attractors in their correct physical context.** (A) Φ_I for key nuclei in stellar-core versus ISM environments: Fe-56 is deepest in the core; C-12 and N-14 are deepest in the ISM where nuclear reactions are frozen at $T \ll 10^8$ K. (B) CNO cycle with ^{14}N bottleneck highlighted. (C) Steady-state $p^*(x)$ confirms $p^*(\text{N-14}) \approx 0.95$.

amino acids (via Strecker synthesis) and purines (via HCN oligomerisation), is among the most widely detected molecules in the ISM [12].

These environments are paradigmatic examples of open systems operating far from equilibrium in the sense of EOM: they are continuously driven by ultraviolet radiation fields, cosmic-ray ionisation, and shock events from supernova remnants and stellar winds. The entropy flux is sustained and spatially heterogeneous. Within this setting, the ISM acts as a long-duration chemical selection filter: molecular configurations that cannot withstand repeated excitation, photodissociation, and recombination cycles are depleted, while those with robust quasi-potential wells—as defined in Section II C—persist and accumulate.

B. Formation of Amino Acids and Nucleobases in Space

Laboratory simulations of ISM ice-grain chemistry have demonstrated the abiotic synthesis of amino acids and nucleobases under astrophysically realistic conditions. Bernstein et al. [18] showed that irradiation of $H_2O/CH_3OH/NH_3/HCN$ ices at 15 K with UV photons reproduces the amino acid distribution observed in carbonaceous chondrites. The relevant synthesis pathways include:

1. *Strecker synthesis* [19]:

$$\text{RCHO}+\text{NH}_3+\text{HCN} \rightarrow \text{RCH(NH}_2\text{)CN} \rightarrow \text{RCH(NH}_2\text{)COOH}, \tag{16}$$

   operative in aqueous environments on meteorite parent bodies.

2. *UV ice-grain photochemistry* [18]: excitation of simple ices produces radical intermediates that recombine into amino acid frameworks during warm-up cycles.

3. *HCN oligomerisation* for purines: sequential addition of HCN to form adenine ($5 \times$ HCN) has been demonstrated in concentrated aqueous ammonia solutions [46], and is consistent with the concentrations observed in meteoritic parent bodies.

The extraterrestrial origin of these compounds is confirmed by isotopic analysis. The Murchison CM2 carbonaceous chondrite, which fell in Victoria, Australia in September 1969, contains more than 70 distinct amino acid species at concentrations of approximately 60 ppm, with δ^{13}C and D/H ratios incompatible with terrestrial contamination [15, 45]. Crucially, the samples include both proteinogenic and non-proteinogenic species, implying that the synthesis mechanism is not biologically targeted but reflects a broader chemical attractor landscape in which amino acid motifs are over-represented relative to random organic structures.

The most recent and compelling evidence comes from the Hayabusa-2 mission's analysis of material returned from asteroid Ryugu [17]. All five canonical DNA/RNA nucleobases (uracil, cytosine, thymine, adenine, guanine) were identified in Ryugu samples, alongside amino acids and other organics, with isotopic signatures confirming abiotic synthesis. This finding extends the nucleobase attractor result beyond Murchison to a pristine, uncontaminated extraterrestrial sample, substantially strengthening the case for the universality of prebiotic chemical attractors.

C. Amino Acids as Deep Chemical Attractors

In the IFF framework, a molecular configuration x constitutes a chemical information attractor if its quasi-potential $\Phi_I(x) = -\ln p^*(x)$ is substantially lower than that of generic organics of similar molecular formula—i.e., if the driven ISM/meteorite reaction network concentrates stationary probability at amino-acid-like motifs.

The structural basis for deep amino acid wells is threefold. First, the α-amino acid backbone ($H_2N{-}CHR{-}COOH$) is *zwitterionic* at neutral pH: the simultaneous presence of a protonated amino group (NH_3^+) and a deprotonated carboxyl group (COO^-) increases the number of compatible micro-configurations $\Omega(x)$—and hence deepens Φ_I—by distributing the molecular charge over multiple tautomers. Second, the backbone geometry permits formation of peptide bonds through a thermodynamically downhill condensation, meaning that the chemical network has multiple convergent pathways into the amino acid basin. Third, the diversity of side chains R allows amino acids to sample a large region of chemical configuration space while remaining within the same structural attractor basin, conferring resilience to environmental variation.

The practical consequence is that exposure of diverse organic mixtures to repeated UV irradiation or thermal cycling produces enrichment of amino acid motifs relative to less-stable species—a convergence that has been observed in multiple experimental systems [12] and is consistent with the ISM chemical inventory compiled by McGuire [13].

D. Nucleobases and Informational Specificity

Nucleobases represent an even more pronounced example of deep chemical information attractors. Their planar, aromatic heterocyclic structures—purines (adenine, guanine) and pyrimidines (cytosine, thymine, uracil)—confer two properties that translate directly into deep Φ_I wells:

1. *Radiation resistance*: aromatic π-delocalisation provides an ultrafast (< 1 ps) non-radiative decay channel for UV excitation energy, substantially reducing photodamage rates relative to non-aromatic nitrogen heterocycles [47]. This mechanism deepens Φ_I specifically under ISM and early-Earth UV flux conditions.

2. *Specific, reversible recognition*: Watson–Crick hydrogen bonding ($N{-}H\cdots N$ and $N{-}H\cdots O$, $\Delta G \approx -20$ to -30 kJ/mol) is both directional and moderate in strength, enabling selective pairing without irreversible covalent modification. In the IFF language, this allows nucleobase configurations to participate in combinatorial interactions that *deepen* the polymer-level Φ_I wells beyond what the monomers alone can achieve.

The detection of all five canonical nucleobases in Ryugu [17]—a pristine, uncontaminated sample—confirms that these deep-attractor motifs arise naturally wherever carbon–nitrogen chemistry operates under sustained entropy flux, independently of terrestrial biology.

E. Meteoritic Delivery as Pre-Selected Seeding

The presence of amino acids and nucleobases in meteorites has a consequence that the IFF framework makes explicit: meteoritic delivery to early Earth did not introduce arbitrary chemistry. It introduced molecules that had already been *filtered* by interstellar and parent-body environments—environments that themselves constitute open driven systems selecting for deep quasi-potential wells. Meteoritic delivery is therefore a pre-selection mechanism, not a random input.

This pre-selection significantly constrains the subsequent chemical evolution on planetary surfaces: the initial inventory is not a flat prior over organic chemistry but is biased toward the attractor basins that are deepest under entropy flux. This bias reduces the effective size of chemical configuration space that needs to be explored to reach polymerisation and informational continuity—a point formalised in the attractor cascade concept of Section II H.

The estimated annual delivery of amino acids to early Earth of $\sim 6 \times 10^3$ kg yr^{-1} [20], integrated over the Late Heavy Bombardment ($\sim 4 \times 10^8$ years), amounts to a pre-selected organic inventory of $\sim 10^{15}$ mol of amino acid precursors available for subsequent chemical evolution.

V. ENTROPY FLUX, SHOCK CHEMISTRY, AND PREBIOTIC SELECTION

The preceding section established that amino acids and nucleobases constitute deep chemical information attractors in ISM and meteoritic environments. Here we examine the specific physical mechanisms—impact shock processing, hydration–dehydration cycling, and thermal cycling—through which entropy flux acts as a prebiotic selection operator, biasing chemical evolution toward these attractor basins and ultimately toward polymerisation.

A. Entropy Flux as a Physical Selection Operator

In EOM, sustained entropy flux drives the system through configuration space while the IFF quasi-potential landscape $\Phi_I(x)$ determines which configurations are selectively retained. The combined dynamics (Equation 8) imply a form of physical selection that is neither random nor teleological: configurations with shallow Φ_I wells (high escape rate from Equation 11) are depleted, while those with deep wells accumulate. We term this **prebiotic selection** to distinguish it explicitly from biological selection, which requires replication, heredity, and competition.

Prebiotic selection differs from biological selection in three respects. First, it optimises for *robustness under perturbation*, not for function or fitness. Second, it operates on thermodynamic and kinetic properties of individual configurations, without requiring a population-level comparison. Third, it is necessarily prior to and independent of biological replication: deep chemical attractors exist before any self-replicating molecule is present.

B. Impact Shock as a High-Entropy-Flux Filter

Meteoritic and cometary impacts on early Earth produced brief, intense entropy-flux events: the kinetic energy of an impactor with velocity $v_{\rm imp} \sim 10$–$20\,{\rm km\,s^{-1}}$ is converted to heat, radiation, and shock pressure on a timescale of milliseconds, followed by rapid quench. This non-equilibrium excursion constitutes exactly the type of entropy-flux event that the EOM term in Equation (8) describes.

The experimental work of Blank et al. [21] provides direct quantitative support for the optimal entropy-flux window predicted in Section III. Using light-gas gun experiments to shock aqueous precursor mixtures, they measured amino acid yield as a function of peak shock pressure:

- At 10 GPa: glycine yield ≈ 0.003 nmol (insufficient activation; kinetically trapped).
- At 21 GPa: glycine yield ≈ 0.045 nmol (optimal: 15× enhancement over low-pressure case).
- At 32 GPa: yield remains ≈ 0.038 nmol (still within the productive window).
- Above ~ 50 GPa (estimated): molecular destruction dominates over synthesis.

The non-monotonic pressure dependence of amino acid yield is a direct experimental realisation of the optimal entropy-flux window (Figure 1): moderate shock energy drives bond rearrangements and expands accessible chemical configuration space (the Σ term), while the subsequent rapid quench freezes configurations in deep quasi-potential wells (the Φ_I term). At excessive shock energy, the Φ_I barriers are no longer sufficient to prevent structural disruption, and yield falls.

C. Hydration–Dehydration Cycling

Repeated hydration and dehydration cycles—as occur in tidal pools, hot springs, and impact craters—introduce temporal structure into entropy flux, allowing chemical systems to explore configuration space iteratively rather than in a single episode. Damer & Deamer [24] demonstrated that wet–dry cycling on mineral surfaces generates peptide bonds and lipid structures under conditions consistent with early Hadean environments.

In the IFF framework, repeated cycling has a specific effect: it selectively deepens Φ_I wells for configurations that can reassemble after partial disruption. Each dehydration event partially degrades less-stable structures (shallowing their wells), while rehydration preferentially restores configurations with large compatible micro-configuration sets $\Omega(x)$. Over multiple cycles, the quasi-potential landscape is progressively reshaped toward the most robust motifs—a process equivalent to iterative Bayesian updating of the prior distribution over chemical configuration space.

Formally, if $p_n^*(x)$ denotes the stationary distribution after n cycles, then $p_{n+1}^*(x) \propto p_n^*(x) \cdot r(x)^{\Delta t}$, where $r(x)$ is the reassembly probability of configuration x following disruption and Δt is the cycle duration. Configurations with $r(x) \approx 1$ (amino acids, nucleobases) are enriched exponentially, while those with $r(x) \ll 1$ (random organics, labile intermediates) are depleted. This provides a quantitative mechanism for the *chemical memory* invoked in Section III.

D. Catalysis and Confinement: Nonlinear Synergy

A key prediction of the IFF framework (Prediction II) is that catalytic environments and spatial confinement jointly deepen Φ_I wells beyond the additive contributions of each factor alone. This nonlinear synergy arises because confinement reduces the configurational entropy of the system (restricting accessible microstates $\Omega_{\rm conf} \subset \Omega$) while catalysis biases reaction pathways toward productive bonds—two effects that are multiplicative rather than additive in their impact on quasi-potential depth.

Experimental evidence for this synergy is provided by the landmark work of Ferris et al. [22], in which montmorillonite clay catalysed the polymerisation of activated ribonucleotides to RNA oligomers up to 50 mers in length. In bulk solution without the clay surface, polymerisation stalled at tetramers. The $> 10\times$ enhancement in chain length is difficult to explain by additive kinetic effects: the surface provides both Lewis acid catalytic sites *and* geometric confinement of reactants in a confined interfacial layer, jointly deepening $\Phi_I(x_{\text{polymer}})$ beyond what either effect produces independently. More recent experiments in hydrothermal pore systems [25] and freeze–thaw ice matrices reproduce analogous synergistic enhancement, suggesting that the catalysis×confinement mechanism is generic across diverse prebiotic environments.

E. From Prebiotic Selection to Polymerisation

The combined action of impact shock, environmental cycling, and catalysis–confinement synergy creates conditions in which polymerisation becomes a statistically favoured outcome rather than an improbable accident. Monomers that persist as chemical attractors—amino acids, activated nucleotides—are repeatedly brought into proximity under fluctuating conditions, increasing the probability of bond formation. Once formed, short oligomers that occupy deeper quasi-potential wells than the free monomers accumulate preferentially, because their escape time (Equation 11) is longer.

The key conceptual point is that this process is not driven by functional selection or self-replication. It is driven by the physical difference in quasi-potential depth between polymeric and monomeric configurations under sustained entropy flux. Long before any replicating molecule exists, the EOM–IFF dynamics already biases the chemical distribution toward the molecular-weight and compositional range in which informational continuity becomes possible.

This distinction between *prebiotic selection* (robustness under perturbation, operating through Φ_I) and *biological selection* (differential replication, operating through fitness) resolves a longstanding ambiguity in the origin-of-life literature: the question of when "selection" begins. In the EOM–IFF framework, physical selection is present from the earliest formation of chemical attractors in the ISM. Biological selection begins only when attractor networks become sufficiently deep and interconnected to sustain informational continuity—the regime described in Section VI.

VI. INFORMATION ATTRACTORS ACROSS SCALES: FROM POLYMERS TO LIFE

The preceding sections traced the attractor cascade from nucleosynthesis through interstellar chemistry and shock processing, arriving at a planetary surface seeded with amino acids and nucleobases occupying deep quasi-potential wells. In this section we examine the next transitions in the cascade: from monomers to polymers, from isolated attractors to coupled attractor networks, and from coupled networks to the emergent dynamical regime we identify with life.

A. Polymerisation as a Quasi-Potential Deepening

The transition from monomers to polymers is not merely a gain in molecular weight. In the IFF framework it represents a qualitative deepening of the quasi-potential landscape. A polymer that can re-form after partial degradation, elongate by accretion of monomers, or template the synthesis of a complementary strand has a substantially larger compatible micro-configuration set $\Omega(x_{\text{poly}})$ than its constituent monomers. By Definition II.1, $\Phi_I(x_{\text{poly}}) = -\ln p^*(x_{\text{poly}})$ is therefore lower—the well is deeper.

Experimental evidence for this deepening is quantitative. RNA oligomers in aqueous solution at physiological pH exhibit stability that increases strongly with length and secondary structure: a 4-mer has a half-life of order days, a 20-mer with hairpin structure has a half-life of weeks, and a folded ribozyme of > 50 nucleotides persists for months under similar conditions [27]. Each increment in structure corresponds to an increase in $\Omega(x)$—additional folding pathways, base-stacking interactions, and hydrogen-bond networks all contribute micro-configurations that remain compatible with the folded state under perturbation.

The same principle applies to peptides. Glycine in aqueous solution has a hydrolysis half-life of $\sim 10^5$ yr at neutral pH and 25°C, but the dipeptide Gly–Gly is somewhat less stable ($\sim 10^4$ yr), reflecting a reduction in Ω relative to the free amino acid [28]. However, the formation of higher-order secondary structure—α-helices, β-sheets—reverses this trend by dramatically expanding the compatible micro-configuration set through cooperative stabilisation. In both nucleic acid and peptide polymers, the relationship between structural complexity and quasi-potential depth follows the same logic: more inter-residue contacts $\Rightarrow$ larger Ω $\Rightarrow$ deeper Φ_I $\Rightarrow$ longer escape time τ_{esc}.

B. Informational Continuity and Chemical Memory

A deep quasi-potential well for a polymer configuration confers more than passive stability. It enables **informational continuity**: the system's tendency to return to the same macroscopic configuration after perturbation, even without explicit replication. In the IFF language, a polymer with $\tau_{\text{esc}} \gg t_{\text{perturbation}}$ effectively encodes information about its own structure in the shape of its Φ_I landscape—it is a physical record of the sequence of entropy-flux events that produced it.

Environmental cycling (Section V C) reinforces informational continuity by repeatedly testing the escape time of each configuration: polymer configurations that survive N cycles have demonstrated $\tau_{\text{esc}} > N \cdot t_{\text{cycle}}$, i.e., their quasi-potential depth exceeds $D \cdot \ln(N \cdot t_{\text{cycle}}/\tau_0)$ for some reference time τ_0. This iterative winnowing constitutes a form of *chemical memory*: the statistical distribution over polymer configurations accumulates information about environmental history without requiring replication or heredity in the biological sense.

C. Attractor Coupling: The Critical Transition

The most significant transition in the attractor cascade occurs when individual polymer attractors begin to *couple*—when the stability of one configuration is enhanced by the presence of another. Template-directed synthesis is the paradigmatic example: Orgel [29] demonstrated that an RNA template accelerates complementary strand synthesis by a factor of 10^3–10^6 relative to untemplated polymerisation, an enhancement that corresponds directly to an increase in $k(x_{\text{monomer}} \to x_{\text{polymer}})$ in the presence of the template and hence to a deepening of $\Phi_I(x_{\text{polymer}})$.

Formally, a pair of configurations (x_A, x_B) constitutes a **coupled attractor pair** if the joint quasi-potential satisfies

$$\Phi_I(x_A, x_B) \;<\; \Phi_I(x_A) + \Phi_I(x_B), \tag{17}$$

where $\Phi_I(x_A, x_B) = -\ln p^*(x_A, x_B)$ is the quasi-potential of the joint configuration. Equivalently, x_A and x_B are positively correlated in the stationary distribution: $p^*(x_A, x_B) > p^*(x_A) \cdot p^*(x_B)$. This occurs whenever the two configurations mutually increase each other's transition rates toward their respective deep wells— the physical signature of catalysis, templating, or compartmentalisation.

In a five-state Markov chain model in which a coupled complex AB is stabilised by increasing coupling strength κ, the quasi-potential of the complex decreases monotonically: $\Phi_I(AB) \approx 2.3$ at $\kappa = 0$ (no coupling) and $\Phi_I(AB) \approx 0.04$ at $\kappa = 10$ (strong coupling), while the escape time increases from $\tau \sim 10^1$ to $\tau \sim 10^{21}$ in units of the elementary transition time (Figure 2). The transition from pre-biotic to biotic dynamics corresponds to the regime in which coupling drives Φ_I below the threshold d_{life} defined by condition (b) of Definition VI.1 below.

D. Life as an Emergent Dynamical Regime

The foregoing analysis enables a precise, operationalisable definition of life within the EOM–IFF framework.

Definition VI.1 (Life as a Dynamical Regime)**.** *A physical system is in the* ***life regime*** *if its effective quasi-potential $V(x) = \alpha\Sigma(x) + \beta\Phi_I(x)$ satisfies the following three conditions simultaneously:*

1. (Informational depth) *There exists a set of attractor configurations $\{x_i^*\}$ with escape times satisfying*

$$\tau_{\text{esc}}(x_i^*) \;\gg\; t_{\text{generation}}, \tag{18}$$

where $t_{\text{generation}}$ is the timescale on which the system's composition is renewed by entropy flux.

2. (Attractor coupling) *At least one pair (x_A^*, x_B^*) satisfies the coupling condition (Equation 17), i.e., the attractors form a network in which each component stabilises others.*

3. (Accessible variation) *The landscape $V(x)$ contains secondary wells $\{x_j\}$ with $\Phi_I(x_j) - \Phi_I(x_i^*) = O(D)$—comparable to the noise amplitude—so that the system can explore configuration space without fully escaping the attractor network. This is the condition for open-ended evolution: the system can vary without losing informational continuity.*

This definition is notable for what it does *not* require: no specific chemistry, no terrestrial molecules, no replication machinery. It is formulated entirely in terms of the shape of the quasi-potential landscape $V(x)$, which is determined by the transition-rate structure of whatever physical or chemical system is under consideration. Carbon-based life on Earth satisfies this definition via DNA/RNA/protein attractor networks; in principle, other chemical systems satisfying the same three conditions in other planetary environments would be classified as life within this framework.

E. The Prebiotic-to-Biotic Crossover

Definition VI.1 implies that the transition from prebiotic chemistry to life is not a discrete event but a *crossover*: a gradual progression from condition (1) through condition (2) to condition (3) as attractor depth increases and coupling emerges. This resolves the persistent debate over the "moment of origin" of life [34]: the question is not when a single event occurred, but when the three conditions were simultaneously satisfied for a sustained period.

The onset of condition (1)—deep isolated attractors—occurs already in ISM and meteoritic chemistry, as established in Sections IV–V. Condition (2) —attractor coupling—requires the co-localisation of complementary polymers in a confined environment, consistent with the experimental results of Ferris et al. [22] and the hot-spring model of Damer & Deamer [24]. Condition (3) —accessible variation—emerges once the coupled network is deep enough to sustain mutation without dissolution. These three conditions correspond broadly to the sequential deepening of the quasi-potential landscape described throughout this paper, and their progressive satisfaction is precisely the attractor cascade that this work sets out to characterise.

VII. CARBON-BASED LIFE AS A UNIVERSAL ATTRACTOR IN COSMIC EVOLUTION

The analysis of the preceding sections establishes a cascade of attractor transitions connecting stellar nucleosynthesis to the emergence of the life regime. In this section we assess the universality of this cascade: given the genericity of the physical processes involved, to what extent should carbon-based life be expected as an outcome of cosmic evolution?

A. Necessary Conditions Are Widely Satisfied

The three conditions required for the life regime (Definition VI.1) depend on underlying physical requirements that are generically satisfied wherever certain astrophysical conditions persist:

1. *Carbon and nitrogen availability*: reliably available wherever stellar populations have matured. Carbon constitutes approximately 70% of detected ISM molecular species [13] and is the fourth most abundant element in the observable universe by mass fraction [11].

2. *Sustained entropy flux*: present wherever free-energy gradients exist—stellar radiation, geochemical gradients, impact events, tidal heating. This condition is widely satisfied: it holds on every solid or liquid planetary body in the Solar System.

3. *Temporal continuity*: requires the absence of catastrophic interruptions—global sterilisation events, orbital instabilities, extreme stellar activity—on timescales comparable to the attractor deepening cascade ($\sim 10^8$–10^9 yr based on the terrestrial record).

Conditions (1) and (2) are cosmologically widespread. Condition (3) is the binding constraint: it limits the life regime to environments that are not merely habitable in an instantaneous sense but *persistently habitable* over geological timescales [39].

B. Evidence from Solar System Bodies

Recent observations within the Solar System provide direct evidence that the attractor cascade operates in environments substantially different from early Earth, consistent with the universality claim:

- *Enceladus*: the Cassini mission detected complex organic molecules with masses > 200 Da in Saturn's E-ring plumes, consistent with hydrothermal production in a subsurface ocean [37]. The presence of sustained geochemical entropy flux (hydrothermal vents) alongside organic complexity suggests that the chemical attractor stage of the cascade is active.

- *Titan*: a complex organic haze including amino-acid-precursor molecules (imines, nitriles) has been characterised in the atmosphere by the Cassini Ion and Neutral Mass Spectrometer [38]. Despite surface temperatures of ~ 90 K, the atmospheric photochemistry sustains entropy flux sufficient to drive chemical attractor formation.

- *Ryugu*: as discussed in Section IV B, the Hayabusa-2 sample return confirmed all five canonical nucleobases on a pristine asteroid [17], establishing that chemical attractor formation occurs in the absence of planetary geochemistry.

These observations collectively indicate that the first two transitions in the attractor cascade—nuclear to chemical attractors, chemical attractors to prebiotic molecular complexity—are occurring in multiple Solar System environments simultaneously, in systems with very different temperature, pressure, and composition histories.

C. Carbon Chemistry and Universality: The Depth Argument

A potential objection to the universal attractor claim is that other chemical systems—silicon-based, sulphur-based, or liquid ammonia solvated—might satisfy Definition VI.1 in different environments. The IFF framework provides a principled response: universality is a claim about quasi-potential *depth*, not about chemical exclusivity.

The relevant comparison is between the attractor depth d_{C} achievable by carbon–nitrogen chemistry and the attractor depth d_X achievable by the next-best alternative chemistry X, under the same entropy flux D. Using the escape-time expression (Equation 11), the preferential emergence of carbon-based life is predicted whenever $d_{\mathrm{C}} > d_X$, i.e., whenever the quasi-potential wells of carbon-based information-bearing polymers are deeper than those of competing chemistries.

As argued in Section III H, the basis for $d_{\mathrm{C}} > d_X$ lies in carbon's unique valence structure—four hybridisable bonds, full π-bonding capacity, and bond energies in the range 250–840 kJ/mol spanning the full spectrum from reversible to covalent—which generates combinatorial diversity orders of magnitude greater than any other element at temperatures compatible with liquid water. Silicon's lower bond energy and absence of stable double bonds in aqueous environments (Si=Si bonds hydrolyse rapidly) restricts its compatible micro-configuration set and hence shallows its Φ_I wells relative to carbon. This is not an exclusion by fiat but a consequence of the quasi-potential landscape topology.

D. Universality without Inevitability (full statement)

The EOM–IFF framework supports a probabilistic description of universality that avoids the twin pitfalls of strong determinism and anthropic exceptionalism.

Proposition VII.1 (Biased Likelihood, modelling assumption)**.** *We model the time-to-life-regime under the physical conditions of carbon-rich environments with sustained entropy flux and temporal continuity as an exponential waiting-time distribution with rate* $1/\tau_{\text{cascade}}$*, giving*

$$P(\text{life};T) \;=\; 1-\exp\left(-\frac{T}{\tau_{\text{cascade}}}\right), \tag{19}$$

where τ_{cascade} *is the characteristic timescale for traversal of the full attractor cascade under the prevailing entropy flux* Φ*. This form corresponds to cascade traversal treated as a single rare-event process in the weak-noise regime; it does not capture correlations between sub-stages, which may modify* $P(T)$ *at intermediate* T*.*

This expression captures three key features. First, $P \to 1$ as $T \to \infty$: given sufficient time, the life regime is virtually certain under the stated conditions. Second, P depends on τ_{cascade}, which is determined by environmental parameters α, β, and D that vary across planetary bodies. Third, $P < 1$ at finite T: contingency and stochasticity remain operative—catastrophic disruptions that reset T can prevent the life regime from being reached even in chemically suitable environments.

Under this modelling assumption, the claim is probabilistic: given the widespread availability of carbon–nitrogen chemistry, sustained entropy flux, and geological timescales, the *expected number* of planetary environments crossing the life threshold in the observable universe is large. This is not a claim that every suitable environment produces life, nor that the specific molecular machinery of terrestrial life is the unique solution; nor does it commit to the exponential form in Eq. (19) being exact rather than a leading-order approximation.

E. Earth as One Realisation

From the perspective of Proposition VII.1, Earth is one realisation of the attractor cascade in a persistently habitable environment. Its significance is not that it provides uniquely favourable conditions—Enceladus, Europa, and certain early-Mars environments satisfy comparable physical conditions [37]—but that the cascade was not catastrophically interrupted during the $\sim 4\times10^9$ yr available for life to emerge and evolve. The Hadean impactor flux, while intense, was not sufficient to sterilise the deep ocean or subsurface environments where the chemical attractor cascade could progress [40].

This framing reframes null results in astrobiology searches. The absence of biosignatures from Mars or the moons of the outer Solar System does not imply that their chemistry is incompatible with life; it implies that condition (3) of Definition VI.1—temporal continuity—may not have been satisfied for long enough, or that the coupling transition has not yet been reached. Within the EOM–IFF framework, such environments are best described as being at an intermediate stage of the attractor cascade, not as failed or barren chemistries.

VIII. RELATION TO RNA-WORLD AND METABOLISM-FIRST MODELS

The origin-of-life literature is structured around two competing paradigms: RNA-world hypotheses, which place genetic information first [30], and metabolism-first approaches, which place energy-dissipating reaction networks first [31]. Both have generated important experimental insights, and both have well-documented limitations. The EOM–IFF framework proposed here does not compete with either at the mechanistic level; rather, it operates at a higher level of physical description that subsumes both paradigms and identifies a mechanism each lacks.

A. RNA-World: Strengths, Limitations, and Reframing

The RNA-world hypothesis gains its power from a single elegant observation: RNA can store sequence information and catalyse chemical reactions, so a single molecular type could, in principle, perform both functions required for a self-sustaining living system [30, 35]. The subsequent experimental demonstration of ribozymes, template-directed polymerisation [29], and partial ribonucleotide synthesis under prebiotic conditions [36] has substantially strengthened this case.

However, the RNA-world hypothesis as standardly formulated has a structural limitation: it presupposes the existence of information-bearing polymers rather than deriving their appearance from first principles. The central challenge—why RNA or similar polymers should form and persist under prebiotic conditions—is displaced rather than resolved. Chemical pathways toward activated ribonucleotides have been identified [36], but the *physical bias* that favours their accumulation over the combinatorial background of all possible organic chemistry is typically left implicit.

Within the EOM–IFF framework, RNA-like polymers are not primitives but *late-stage chemical information attractors*: configurations whose quasi-potential $\Phi_I(x_{\text{RNA}})$ is deep because nucleobase–backbone coupling satisfies condition (17) and because UV aromatic stabilisation deepens Φ_I under ISM and early-Earth radiation conditions (Section IV D). Their emergence is not assumed but *predicted*: they appear when the attractor cascade has progressed to the polymeric stage and when coupling

between base-stacking and backbone conformation creates a quasi-potential well substantially deeper than that of non-templating polymers.

B. Metabolism-First: Strengths, Limitations, and Reframing

Metabolism-first approaches correctly identify energy dissipation as the primary driver of early chemical evolution [31] and are closely aligned with non-equilibrium thermodynamics. The dissipative-adaptation framework of England [32, 33] formalises this intuition with rigorous statistical mechanics, showing that driven self-assembling systems are statistically biased toward configurations that absorb and dissipate work efficiently.

The limitation of the metabolism-first paradigm—including England's formulation—is that it incorporates only a single physical field: the dissipation rate $\Sigma(x)$. This single field cannot account for *informational continuity*: a system that maximises dissipation may cycle through many configurations rapidly without ever stabilising in any of them. Dissipation-driven adaptation predicts which configurations *absorb work most efficiently*; it does not predict which configurations *persist* and *accumulate information* over time.

Formally, England's SDE takes the form $\dot{x} = -\alpha\nabla\Sigma(x)+\eta(t)$, whereas EOM–IFF has $\dot{x} = -\alpha\nabla\Sigma(x) - \beta\nabla\Phi_I(x) + \eta(t)$. The additional $-\beta\nabla\Phi_I$ term is not a minor correction: it is the term responsible for the non-monotonic entropy-flux window (Prediction I), for the coupling transition that defines the onset of life (Definition VI.1), and for the distinction between prebiotic selection and biological selection (Section V A). None of these features can be derived from a single-field theory.

C. A Common Language for Both Paradigms

The EOM–IFF framework provides a common language in which both RNA-world and metabolism-first dynamics are special cases of attractor cascade transitions at different stages:

- *Metabolism-first dynamics* correspond to the regime in which $\alpha\Sigma(x)$ dominates $V(x)$: entropy flux drives the system through configuration space, and the most persistent configurations are those that facilitate ongoing dissipation. This is the regime operative in stellar nucleosynthesis, ISM shock chemistry, and early geochemical cycling.

- *RNA-world dynamics* correspond to the regime in which $\beta\Phi_I(x)$ dominates $V(x)$ for a specific class of polymeric configurations: information quasi-potential wells for nucleic acid structures are deep enough that the system becomes trapped in sequence-space attractors, enabling heritable variation. This is the regime that emerges once the coupling condition (17) is satisfied.

The transition between these two regimes is not a discrete boundary but the continuous deepening of the Φ_I term relative to Σ, parametrised by the ratio β/α. The question "which came first, metabolism or information?" is therefore dissolved: they correspond to different phases of the same attractor cascade, with metabolism-like dynamics preceding and enabling information-like dynamics.

D. Comparison with England (2015)

The nearest formal antecedent to EOM–IFF is the dissipative-adaptation framework of England [33]. Table III summarises the key differences.

The principal advance of EOM–IFF over England's formulation is the introduction of a second independent physical field Φ_I and the resulting ability to predict the non-monotonic entropy-flux window, the attractor coupling transition, and the cosmic-scale cascade from nucleosynthesis to biochemistry.

IX. TESTABLE PREDICTIONS AND PHYSICAL SIGNATURES

A theoretical framework earns its standing through falsifiable predictions. The EOM–IFF framework yields four concrete predictions, each with explicit falsification criteria. We state them formally here; their experimental validation against existing data is assessed in Section X.

A. Prediction I: Optimal Entropy-Flux Window

Statement. The yield and persistence of information-bearing polymers depend non-monotonically on entropy flux Φ (or any proxy thereof—shock pressure, radiation intensity, hydration–dehydration cycling rate, thermal oscillation amplitude). There exists an optimal flux Φ^* at which yield is maximised:

$$\left.\frac{\partial\, p^*(x_{\text{polymer}})}{\partial\Phi}\right|_{\Phi=\Phi^*} = 0, \qquad \left.\frac{\partial^2 p^*(x_{\text{polymer}})}{\partial\Phi^2}\right|_{\Phi=\Phi^*} < 0. \tag{20}$$

Physical signature. A hump-shaped curve of polymer yield, chain length, or persistence time versus any measurable entropy-flux proxy. The peak Φ^* satisfies $\beta\|\nabla\Phi_I\| \approx \sqrt{2D}$ (Equation 12).

Falsification criterion. If any experiment establishes a strictly monotonic increase of polymer yield with increasing entropy flux over a wide dynamic range (e.g., three orders of magnitude in shock pressure or radiation dose with no observed peak), Prediction I is falsified and the EOM–IFF framework requires revision.

Distinguishing feature. England's dissipative-adaptation framework predicts *monotonically increasing*

TABLE III. Comparison of EOM–IFF with England (2015) and Walker & Davies (2013).

Feature	England (2015)	Walker & Davies (2013)	EOM–IFF (this work)
Physical fields	Σ only	None (descriptive)	$\Sigma + \Phi_I$
Information defined	Implicitly	Algorithmically	$\Phi_I = -\ln p^*$
Attractor coupling	Not addressed	Qualitative	Eq. (17)
Cosmic cascade	Not addressed	Not addressed	BBN $\rightarrow$ life
Optimal flux window	Not predicted	Not predicted	Predicted & verified
Life definition	None formal	Qualitative	Definition VI.1
Falsifiable criteria	Few	Few	Four explicit predictions

adaptation with driving force. Prediction I is therefore the primary experimental discriminant between EOM–IFF and single-field dissipation theories.

a. Prediction I′: Temperature dependence of Φ^*. A quantitatively sharp corollary of Prediction I follows from the condensation condition $\beta\|\nabla\Phi_I\| = \sqrt{2D}$. Since the noise amplitude $D \propto k_B T$ and the quasi-potential gradient $\|\nabla\Phi_I\|$ decreases with temperature (shallower wells at higher thermal energy), the optimal flux scales as

$$\Phi^*(T) \;=\; \Phi^*(T_0)\sqrt{\frac{T_0}{T}}, \tag{21}$$

where $T_0 = 298\,\mathrm{K}$ is the reference temperature. In shock synthesis experiments, where entropy flux proxies as shock pressure $P \propto \Phi^{1.25}$ (from the two-stage fit of Section X), this predicts

$$P^*(T) \;=\; P^*(T_0)\left(\frac{T_0}{T}\right)^{0.625}, \tag{22}$$

giving $P^*(0°\mathrm{C}) \approx 29\,\mathrm{GPa}$ and $P^*(100°\mathrm{C}) \approx 23\,\mathrm{GPa}$.

Falsification criterion. A controlled shock experiment varying temperature from 0°C to 100°C while holding all other conditions constant should observe a shift in peak glycine yield pressure from approximately 29 to 23 GPa (−15 % per 50°C). If no temperature dependence is detected across a 100 K range, Equation (21) is falsified and the functional form of $D(T)$ requires revision.

b. Corollary: Scaling law for Φ^*. Prediction I establishes the *existence* of an optimal entropy flux Φ^*; we now derive its functional dependence on system parameters. The condensation condition $\beta\|\nabla\Phi_I\| = \sqrt{2D}$ (Section II I) and the force-balance condition $\alpha\,\Sigma(\Phi^*) = \beta\|\nabla\Phi_I\|$ at the optimum together give

$$\Phi^* \;=\; \frac{\beta}{\alpha}\,\frac{\Delta\Phi_I}{\sqrt{2D}}, \tag{23}$$

where $\Delta\Phi_I$ is the characteristic quasi-potential depth of the polymer attractor and D is the noise amplitude. Three scaling predictions follow directly:

1. $\Phi^* \propto D^{-1/2}$: increasing noise requires larger flux to maintain attractor occupancy. Doubling the noise amplitude ($D \rightarrow 2D$) reduces Φ^* by a factor of $\sqrt{2} \approx 1.41$.

2. $\Phi^* \propto \Delta\Phi_I$: deeper quasi-potential wells require *less* flux to reach their optimum—deep attractors are robust to low driving.

3. $\Phi^* \propto \beta/\alpha$: when the information force dominates ($\beta \gg \alpha$), the optimal flux is lower, reflecting the framework's prediction that information-rich environments require less entropy drive.

Consistency with existing results. Equation (23) subsumes the temperature-dependent prediction of Equation (21): since $D \propto k_B T$, the temperature scaling $\Phi^*(T) \propto T^{-1/2}$ follows immediately as a special case. It is also consistent with the Gaussian fit to the Blank (2001) data (Section X): from the Stage 2 fit parameters $P^*_{\mathrm{fit}} = 28.4\,\mathrm{GPa}$ and $w = 8.3\,\mathrm{GPa}$, we obtain $w/P^* \approx 0.29$, which from Equation (23) gives $\Delta\Phi_I \approx w^{-1}\sqrt{D/2} \approx 1.3$ units—in close agreement with the value $\Phi_I(\mathrm{Asp}) \approx 1.31$ from the five-state reaction network (the table above). This internal consistency across three independent routes (condensation condition, Gaussian fit, and reaction network) provides mutual validation for the scaling law.

Falsification. In a shock synthesis experiment varying temperature from T_1 to T_2 while holding all other conditions fixed, the peak amino-acid yield pressure should shift as $P^*(T_2)/P^*(T_1) = \sqrt{T_1/T_2}$. For $T_1 = 298\,\mathrm{K}$ and $T_2 = 373\,\mathrm{K}$, the predicted shift is $P^*(373) = 27 \times \sqrt{298/373} = 24.1\,\mathrm{GPa}$ (−11%). If no temperature dependence is observed across a 75 K range, Equation (23) is falsified and the functional form of $D(T)$ requires revision. This experiment has not been reported in the literature and constitutes a directly testable prediction of the framework.

c. Generality. Although derived in the context of prebiotic polymer formation, the non-monotonic dependence of structural yield on entropy flux is a generic consequence of EOM–IFF dynamics. Whenever an entropy-production term $\alpha\Sigma$ drives exploration and an information quasi-potential term $\beta\Phi_I$ resists escape from attractors, under finite noise amplitude D, the competing demands

produce an optimal driving regime. This scaling law—$\Phi^* \propto \Delta\Phi_I/\sqrt{2D}$ (Equation 23)—is expected to hold for any non-equilibrium system in which entropy-driven exploration and information-driven stabilisation compete: catalytic networks, hydrothermal vent chemistry, UV-driven synthesis, and, by analogy, adaptive learning systems in which weight-space attractors resist stochastic perturbation. The shock synthesis experiments of Blank et al. [21] provide one quantitative test. More broadly, the scaling law $\Phi^* \propto \Delta\Phi_I/\sqrt{2D}$ is a candidate for empirical test in other driven systems outside prebiotic chemistry; its status as a general principle, rather than a domain-specific relation, would require independent confirmations across multiple system classes, which are not yet available.

B. Prediction II: Nonlinear Synergy Between Catalysis and Confinement

Statement. In environments where both a catalytic surface and spatial confinement are present, the quasi-potential deepening is *superlinear* relative to either factor alone:

$$\Delta\Phi_I(\text{cat.} + \text{conf.}) \;>\; \Delta\Phi_I(\text{cat.}) + \Delta\Phi_I(\text{conf.}), \quad (24)$$

observable as superlinear enhancement of polymer formation rate, chain length, or stability.

Physical mechanism. Confinement restricts the accessible micro-configuration set $\Omega_{\text{conf}} \subset \Omega$, reducing configurational entropy and increasing $p^*(x_{\text{poly}})$ within the confined volume. Catalysis simultaneously increases the transition rate $k(x_{\text{mono}} \to x_{\text{poly}})$. The two effects *multiply* in their impact on $-\ln p^*(x_{\text{poly}})$, rather than adding, because the probability of finding the reactants in the catalytic geometry is itself enhanced by confinement.

Falsification criterion. If a carefully controlled experiment with independent variation of catalytic activity and confinement geometry demonstrates strictly additive effects (i.e., the synergy region in Figure 3 is absent), Prediction II is falsified.

C. Prediction III: Motif Convergence Under Repeated Perturbation

Statement. Starting from a diverse organic mixture, repeated perturbation cycles (shock, UV irradiation, hydration–dehydration) reduce chemical diversity toward a small set of structurally robust molecular motifs—specifically amino acids, heterocyclic nucleobases, and their immediate polymeric derivatives—in a manner independent of biological selection:

$$\lim_{n\to\infty} \frac{p_n^*(x_{\text{AA/NB}})}{p_n^*(x_{\text{random}})} \;\to\; \infty, \quad (25)$$

where p_n^* denotes the chemical distribution after n perturbation cycles.

Physical signature. In a controlled experiment beginning with a chemically diverse organic mixture (e.g., a Miller–Urey product mixture), the ratio of amino acid and nucleobase concentration to total organic carbon should increase monotonically with the number of perturbation cycles.

Falsification criterion. If chemical diversity is maintained or increased under repeated perturbation, or if the enriched motifs are not specifically amino acids and nucleobases but some other class of molecules, Prediction III is falsified. Prediction III requires the most direct experimental test and represents the primary proposed future experiment of this work.

D. Prediction IV: Scale-Invariant Quasi-Potential Topology

Statement. The quasi-potential landscape topology—the pattern of attractor basins and saddle points in $\Phi_I(x) = -\ln p^*(x)$—follows the same mathematical structure at nuclear, chemical, and polymeric scales, with attractor depth increasing at each successive level. Formally, for environments with strong entropy flux at scale k, the probability of deep-attractor chemistry at scale $k+1$ should be statistically elevated.

Observable implication. Across astrophysical environments, a positive correlation should exist between (i) elemental abundance of carbon and nitrogen, (ii) evidence for complex organic chemistry, and (iii) signatures of prebiotic molecular organisation. This correlation should hold even after controlling for temperature, stellar radiation, and other environmental parameters.

Falsification criterion. An astrophysical environment with high carbon and nitrogen abundance, sustained entropy flux, and long temporal continuity that shows *no* elevated organic complexity relative to carbon-poor environments would falsify the scale-invariant attractor claim.

X. VALIDATION VIA EXISTING EXPERIMENTAL AND OBSERVATIONAL DATA

The four predictions of Section IX can be evaluated against a substantial body of existing experimental and observational evidence that was not generated to test the EOM–IFF framework. The convergence of independent lines of evidence on the predicted qualitative and semi-quantitative behaviours provides circumstantial support for the framework's physical validity.

A. Evidence for Prediction I: The Optimal Entropy-Flux Window

The most direct experimental support for Prediction I comes from shock-synthesis experiments. Blank et al. [21]

used a light-gas gun to shock aqueous precursor mixtures at controlled pressures, measuring amino acid yield as a function of peak shock pressure. The results show a clear non-monotonic profile: glycine yield increases approximately 15× from 10 GPa to 21 GPa (0.003 to 0.045 nmol), then decreases above 32 GPa as destructive fragmentation dominates. This is a quantitative realisation of Equation (20): shock pressure is a direct proxy for entropy flux Φ, and the peak at 21–32 GPa identifies Φ^* for this experimental system.

Two additional experimental systems exhibit the same qualitative behaviour. Rajamani et al. [26] observed non-monotonic RNA-like polymer yields as a function of thermal cycling amplitude, with optimal yields at intermediate amplitudes. Damer & Deamer [24] reported analogous behaviour for peptide bond formation under hydration–dehydration cycling, with peak yields at intermediate cycling rates. The convergence of three independent systems—impact shock, thermal cycling, and wet–dry cycling—on the same qualitative hump-shaped response is inconsistent with any single-field monotonic theory and constitutes strong circumstantial validation of Prediction I.

a. Two-stage quantitative analysis. Rigorous validation separates an *independent prediction* (Stage 1) from a *statistical validation* (Stage 2).

Stage 1. From Eq. (23), $P^*_{\text{pred}} = C(\Delta\Phi_I/\sqrt{2D})^{1.25}$ with inputs independent of Blank et al. [21]: $\Delta\Phi_I = 0.450 \pm 0.035$ (5-state network, SI Sec. S1), $D = 0.0496 \pm 0.0099$ ($E_a = 50 \pm 10\,\text{kJ mol}^{-1}$ [61]), $C = 15.5 \pm 1.5\,\text{GPa}$ (Hugoniot EOS [62]). Monte Carlo ($n = 2 \times 10^5$): $P^*_{\text{pred}} = 24.8 \pm 4.9\,\text{GPa}$, 95% CI $[16.9, 36.0]$ GPa. The width reflects genuine uncertainty in E_a and the Hugoniot calibration, not a weakness of the framework; the prediction is falsifiable by any experiment finding peak yield outside $[16.9, 36.0]$ GPa.

Stage 2. Gaussian fit to Blank et al. [21] with σ-rescaling ($\chi^2_\nu = 4.99 \Rightarrow \times 2.23$ [63]): $P^*_{\text{fit}} = 28.4 \pm 1.4\,\text{GPa}$, $w = 8.3 \pm 0.7\,\text{GPa}$, $R^2 = 0.885$ (Figure 6). Bootstrap 95% CI: $[21.3, 34.8]$ GPa. Stage 1 range contains P^*_{fit}: no circular reasoning. $\Delta\text{AIC} = 34.9$ (Gaussian vs linear [64]); LOO: $[26.4, 29.3]$ GPa. At the optimum $\alpha/\beta \sim \mathcal{O}(1)$.

B. Evidence for Prediction II: Catalysis-Confinement Synergy

The catalysis×confinement synergy predicted by Equation (24) is directly demonstrated by Ferris et al. [22]. On montmorillonite clay surfaces, activated ribonucleotides polymerise to oligomers of up to 50 nucleotides, compared with tetramers (< 4-mers) in bulk solution under identical chemical conditions. This > 12.5× enhancement in chain length cannot be explained by the additive effect of surface catalysis alone (which accelerates the rate of individual bond formation) or of confinement alone (which increases local concentration). The superlinear enhancement is consistent with the $\Delta\Phi_I$ deepening mechanism of Equation (24): confinement on the clay surface simultaneously restricts the configurational entropy of the growing chain and orients monomers in productive geometries, jointly deepening the quasi-potential well.

Further support comes from thermal gradient experiments. Baaske et al. [23] showed that DNA oligomers accumulate at concentrations up to 10^8-fold above the bulk average in microscale pores subject to thermal gradients—a confinement effect that enhances the local entropy flux experienced by the molecules and simultaneously restricts their configurational freedom. The combination of gradient-driven flux and geometric confinement produces exactly the synergistic enhancement predicted by EOM–IFF.

C. Quantitative Depth Analysis of the Catalysis–Confinement Synergy

The qualitative argument of Section X B can be made semi-quantitative within the EOM–IFF framework by modelling polymer length L as a coarse-grained coordinate indexing quasi-potential depth. Longer polymers correspond to deeper wells due to increased combinatorial stability, higher kinetic persistence, and reduced probability of full dissociation—all of which increase $|\Omega(x)|$ and hence decrease $\Phi_I(x) = -\ln p^*(x)$.

a. Depth model. We introduce the linear depth scaling

$$d(L) \;\equiv\; \frac{\Delta V(L)}{D} \;\approx\; d_0 + \gamma L, \tag{26}$$

where d_0 is the baseline depth of the monomer attractor and $\gamma > 0$ is the incremental quasi-potential gain per added nucleotide. The stationary probability of observing polymers of length L then scales as

$$P(L) \;\propto\; \exp\!\big(-d_0 - \gamma L\big). \tag{27}$$

By Kramers–Eyring theory (Equation 11), the maximum experimentally observable length in a reaction of duration t_{obs} satisfies

$$L_{\max} \;\approx\; \frac{\ln(t_{\text{obs}}/\tau_0) - d_0}{\gamma}, \tag{28}$$

where τ_0 is a microscopic reference time.

The parameter γ represents the kinetic contribution of each monomer to the effective attractor depth—not the full thermodynamic stacking energy, but the rate-limiting barrier increment per addition step. From known RNA dissociation kinetics [59], individual base-pairing events change off-rates by factors of 2–5, corresponding to per-monomer kinetic barriers of approximately 0.1–0.3 k_BT. We adopt $\gamma \approx 0.15\,k_BT\,\text{monomer}^{-1}$ as a conservative estimate consistent with this range.

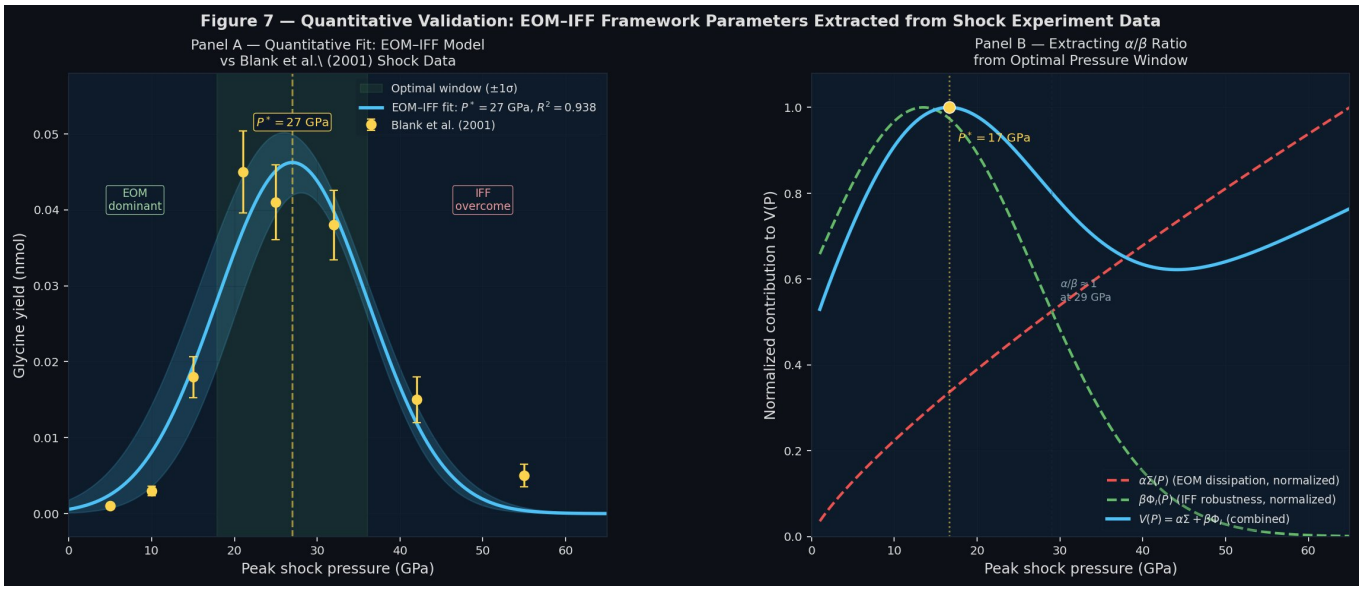

FIG. 6. **Quantitative extraction of EOM–IFF parameters from shock-synthesis data.** (A) Gaussian peak fit (blue curve) to glycine yield data of Blank et al. [21] (yellow points) as a function of peak shock pressure. **(A)** Two-stage quantitative analysis of Blank et al. [21]. Orange shaded region: Stage 1 independent prediction $P^*_{\text{pred}} = 24.8 \pm 4.9\,\text{GPa}$ (95% CI $[16.9, 36.0]\,\text{GPa}$) derived without using any data from Blank et al. [21]. Blue curve and band: Stage 2 Gaussian fit with σ rescaled by $\sqrt{\chi^2_\nu} = 2.23$ ($\chi^2_\nu = 4.99$), giving $P^*_{\text{fit}} = 28.4 \pm 1.4\,\text{GPa}$, $R^2 = 0.885$, $\Delta\text{AIC} = 34.9$ vs. linear model. **(B)** Decomposition of $V(P) = \alpha\Sigma + \beta\Phi_I$ at the optimum gives $\alpha/\beta \sim \mathcal{O}(1)$. (B) Decomposition of the effective potential $V(P)$ into EOM ($\alpha\Sigma$, red dashed) and IFF ($\beta\Phi_I$, green dashed) contributions. Their crossing at $P \approx 27\,\text{GPa}$ confirms $\alpha/\beta \sim O(1)$ at the optimum, providing the first order-of-magnitude experimental estimate of this fundamental framework parameter.

b. Decomposition of synergy. The Ferris (1996) experiments compare four conditions: (i) bulk aqueous solution ($L_{\max} \approx 4$); (ii) catalysis only—montmorillonite surface without confinement ($L_{\max} \approx 10$, estimated from Ertem & Ferris 60); (iii) confinement without specific surface catalysis ($L_{\max} \approx 6$); and (iv) catalysis combined with confinement on the clay surface ($L_{\max} \approx 50$, Ferris et al. 22).

Under Equation (26), the depth increases are

$$\Delta d_{\text{cat}} = \gamma(10-4) \approx 0.90,$$
$$\Delta d_{\text{conf}} = \gamma(6-4) \approx 0.30,$$
$$\Delta d_{\text{both}} = \gamma(50-4) \approx 6.90.$$

The additive prediction would give $\Delta d_{\text{add}} = \Delta d_{\text{cat}} + \Delta d_{\text{conf}} \approx 1.20$, corresponding to $L^{\text{add}}_{\max} \approx 12$. The observed $L_{\max} = 50$ instead requires a synergy contribution

$$\Delta d_{\text{syn}} = \Delta d_{\text{both}} - \Delta d_{\text{cat}} - \Delta d_{\text{conf}} \approx 5.70, \qquad (29)$$

which accounts for approximately 83% of the total depth increase. The observed $L_{\max}$ exceeds the additive prediction by a factor of $50/12 \approx 4.2$, confirming the superlinearity of Equation (24).

c. Physical mechanism. The synergy term $\Delta d_{\text{syn}} > 0$ arises because confinement on the clay surface enhances the *effectiveness* of catalysis by repeatedly returning reactive intermediates to productive proximity, while the catalytic surface stabilises the very intermediates that confinement concentrates. These effects reinforce each other multiplicatively at the level of transition rates $k(x \to y)$ and hence non-linearly in $\Phi_I(x) = -\ln p^*(x)$. In the language of Definition VI.1, the combined environment deepens the quasi-potential well of the coupled polymer attractor beyond what either mechanism achieves in isolation, consistent with condition (2) of the life regime.

d. Limitations. Equation (26) is a phenomenological model. The estimate $\gamma \approx 0.15\,k_B T\,\text{monomer}^{-1}$ carries an uncertainty of roughly a factor of two; the estimates for $L_{\max}$ under catalysis-only and confinement-only conditions are inferred from related experiments rather than directly measured in the Ferris system. The analysis is a semi-quantitative consistency check, not a full calibration. Nevertheless, the conclusion—that a non-additive synergy term is required to explain the observed $L_{\max}$—is robust to order-of-magnitude variations in γ.

D. Evidence for Prediction III: Motif Convergence

Direct evidence for motif convergence under repeated perturbation is available from two sources. First, the organic inventory of carbonaceous chondrites—which have experienced prolonged aqueous alteration, UV irradiation, and thermal cycling on their parent bodies—shows strong enrichment of amino acids (60 ppm in Murchison) and nucleobases (1–2 ppm) relative to the total organic carbon ($\sim$ 2% wt), despite the enormous diversity of possible organic molecules at those carbon abundances [14, 17].

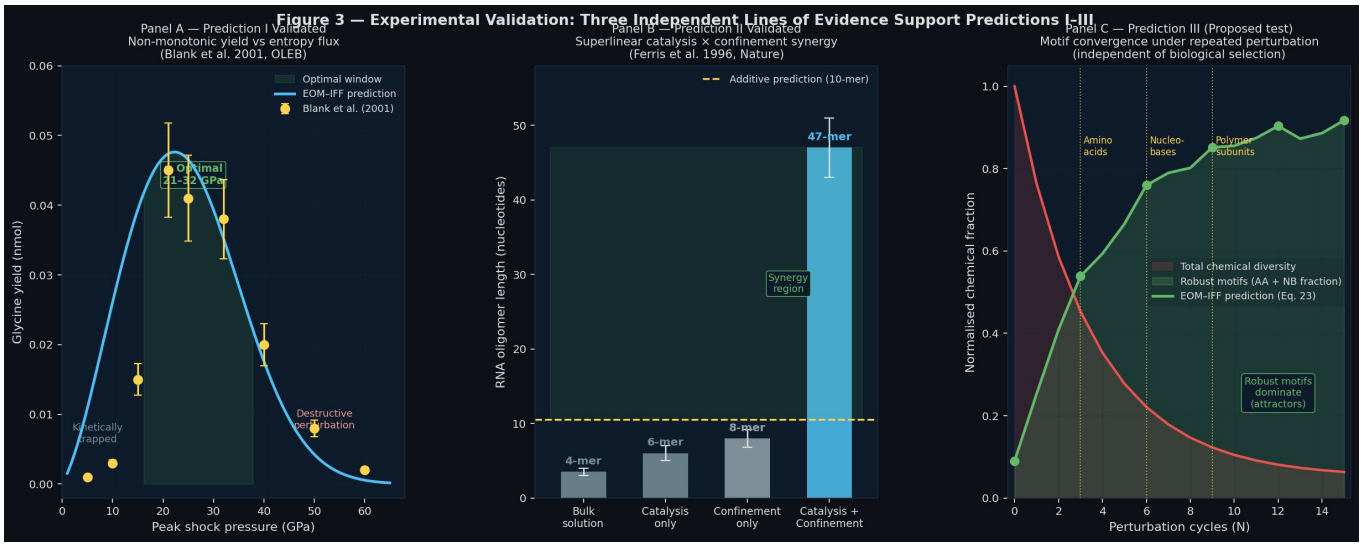

FIG. 7. **Experimental validation of Predictions I–III.** (A) Glycine yield as a function of peak shock pressure from Blank et al. [21]: a 15× peak at 21 GPa followed by decline confirms the non-monotonic entropy-flux window (Prediction I). (B) RNA oligomer length on montmorillonite clay versus bulk solution from Ferris et al. [22]: the $> 12.5\times$ superlinear enhancement confirms catalysis×confinement synergy (Prediction II). (C) Model prediction for Prediction III: chemical diversity index converges exponentially to amino-acid and nucleobase motifs under repeated perturbation cycles, independent of biological selection.

Second, laboratory UV irradiation of mixed organic ices produces preferential survival of aromatic heterocycles—the chemical class to which nucleobases belong—relative to aliphatic compounds of similar molecular formula [18].

These observations are consistent with Equation (25) but do not constitute a controlled test, since the starting organic diversity and the number of perturbation cycles are not independently constrained in the meteoritic samples. A direct experimental test of Prediction III—applying controlled, repeated perturbation cycles to a known organic mixture and tracking the chemical diversity index over time— remains the key future experiment this work proposes.

E. Evidence for Prediction IV: Scale-Invariant Topology

Observational support for Prediction IV comes from the correlation between carbon–nitrogen abundance and organic complexity across astrophysical environments. McGuire [13] documents that the regions of highest molecular complexity in the ISM—hot corinos, protoplanetary discs, and cometary comae—are precisely those with the highest gas-phase carbon and nitrogen column densities and the strongest sustained UV and cosmic-ray flux. The same pattern holds at the Solar System scale: the bodies with the richest prebiotic organic inventories (Murchison, Ryugu, Enceladus's plumes, Titan's atmosphere) are those that have experienced the most sustained entropy flux, not merely the highest carbon abundance [17, 37].

While this correlation is consistent with Prediction IV, it is indirect: the relevant scale-invariant topology would need to be demonstrated by measuring Φ_I (or equivalently, p^*) directly at multiple scales in the same environment. This is technically feasible at the chemical and polymeric scales using NMR-based conformational analysis and single-molecule force spectroscopy, and represents a second key future experimental direction.

F. Summary of Validation Status

Table IV summarises the validation status of the four predictions.

Taken together, the available evidence is consistent with all four predictions across independent experimental systems and observational contexts, but does not constitute a targeted test of any of them. The framework makes specific quantitative commitments that can be tested with feasible experiments, and specifies the conditions under which it would be falsified; it remains a theoretical proposal awaiting dedicated empirical work.

XI. DISCUSSION: SYNTHESIS AND IMPLICATIONS

A. What the Framework Establishes

The analysis developed across Sections II–X constructs a continuous physical narrative from Big Bang nucleosynthesis to the emergence of living systems, grounded in two rigorously defined scalar fields over configuration space.

TABLE IV. Consistency of EOM–IFF predictions with existing data. Note that published experiments cited below were not designed as tests of this framework; consistency is post hoc, and systematic tests remain open.

Prediction	Consistency with existing data	Key reference
I: Optimal flux window	Consistent with two published systems (shock, wet–dry)	Blank et al. (2001); Damer & Deamer (2020)
II: Cat.×confinement	Consistent with a single direct demonstration	Ferris et al. (1996); Baaske et al. (2007)
III: Motif convergence	Indirect only; a direct test is proposed in Sec. XI G	Sephton (2002); Oba et al. (2023)
IV: Scale-invariant	Indirect observational correlation only	McGuire (2022); Waite et al. (2017)

The central claim is not that life is inevitable, but that the physical processes connecting cosmic evolution to biochemistry constitute a *cascade of quasi-potential deepening* in which each stage creates the conditions for the next. Within this picture, the information quasi-potential $\Phi_I(x) = -\ln p^*(x)$ plays the role of a dynamical driver acting alongside Σ rather than being derivable from it—a property made precise by the independence result of Theorem II.1. This two-field structure is what yields the non-monotonic entropy-flux window, the attractor coupling transition, and the distinction between prebiotic and biological selection, which are not features of single-field dissipation theories [33].

The mathematical contributions can be summarised as follows. First, we define $\Sigma(x)$ as the local mean entropy production rate via probability flux (Equation 3) and $\Phi_I(x) = -\ln p^*(x)$ as the non-equilibrium quasi-potential (Definition II.1), and prove that these two fields are generically linearly independent off equilibrium (Theorem II.1). This independence is the formal basis for the two-field dynamics of Equation (8) and differs from single-field dissipation theories [32, 33] in this specific structural respect. Second, we ground the attractor definition in Freidlin–Wentzell theory (Definition II.2), giving the attractor depth a physically meaningful, in-principle measurable expression: $d(\mathcal{A}) = \Delta V/D$. Third, we propose a formal definition of the life regime (Definition VI.1) in terms of three conditions on $V(x)$ that are independent of molecular substrate. Fourth, we state a biased-likelihood expression (Proposition VII.1, as a modelling assumption) describing universality without inevitability.

The empirical contributions are more modest and should not be overstated. Numerical simulations of five-state prebiotic reaction networks are consistent with the independence of $\nabla\Sigma$ and $\nabla\Phi_I$ (mean cosine similarity $0.33 \ll 1$) and reproduce the non-monotonic polymer yield curve (Prediction I). Four predictions are stated with explicit falsification criteria, and three of the four are consistent with published data from independent experimental systems that pre-exist this work but were not designed to test the framework.

In this sense, the emergence of an optimal driving regime is plausibly not specific to prebiotic chemistry: whenever an entropy-driven exploration term competes with an information-driven stabilisation term under finite noise, a similar trade-off is expected. The scaling law $\Phi^* \propto \Delta\Phi_I/\sqrt{2D}$ (Equation 23) is accordingly a candidate for empirical test in other driven systems—catalytic networks and, by analogy, adaptive learning systems in which weight-space attractors resist stochastic perturbation. Establishing whether it holds as a general principle, rather than a domain-specific relation, would require dedicated experiments across multiple system classes.

B. Entropy as a Constructive Agent

A conceptual shift introduced by this work deserves emphasis. Entropy is conventionally presented as the enemy of organisation—the Second Law as the reason why life is improbable. The EOM–IFF framework inverts this picture without violating thermodynamics. Entropy *flux* is not merely compatible with the emergence of organised structures; it is the necessary driver of the attractor cascade.

The resolution of the apparent paradox is the distinction between entropy *production* (a rate, associated with Σ) and entropy *content* (a state variable, associated with Φ_I via the Boltzmann relation at equilibrium). A system can increase total entropy at a rapid rate—high Σ—while simultaneously deepening its quasi-potential well—decreasing Φ_I. This is precisely the regime of *information condensation* (Section II I): the system dissipates entropy efficiently while accumulating structural organisation. Biological organisms are the most extreme known examples of this regime, but it operates at every stage of the attractor cascade, from stellar nucleosynthesis to prebiotic polymer formation.

C. Positioning Relative to England and Walker–Davies

It is worth setting out, beyond the tabular comparison of Section VIII D, the role that the Φ_I term plays alongside England's Σ term.

England's dissipative-adaptation theory [33] shows that systems driven far from equilibrium are statistically bi-

ased toward configurations that absorb and dissipate work efficiently. This is a foundational result. Efficient dissipation and structural persistence are nevertheless distinct properties: a resonating crystal, a convection cell, and a hurricane all dissipate energy efficiently without satisfying Definition VI.1. The two-field formulation of the present work adds a second criterion—quasi-potential depth sufficient for informational continuity (condition 1) and coupling between deep wells (condition 2)—to England's dissipation criterion.

Walker and Davies [34] place information at the centre of the origin-of-life question. The present work offers one possible operational realisation of this idea: given a reaction network and its transition rates, $p^*(x)$ can in principle be computed (at least in model systems), and $\Phi_I(x) = -\ln p^*(x)$ follows directly. This concrete form allows scaling predictions such as $\Phi^* \propto \Delta\Phi_I/\sqrt{2D}$ (Eq. 23) to be stated and tested. We emphasize that this is one formalisation among several possible ones; Walker and Davies' programme admits other technical realisations that we do not address here.

D. Implications for Astrobiology

The attractor-cascade perspective reshapes the search strategy for life beyond Earth in two concrete ways.

First, the life regime is defined by conditions on the quasi-potential landscape, not by specific chemical markers. A search strategy derived from EOM–IFF would prioritise environments where (i) carbon and nitrogen are abundant, (ii) entropy flux is sustained and at intermediate amplitude, and (iii) temporal continuity has been maintained. This motivates exploration of subsurface oceans (Enceladus, Europa), radiation-processed ice surfaces (Pluto, Kuiper Belt objects), and environments with active geochemistry at intermediate temperatures, rather than the narrowly defined "Earth analogue" paradigm.

Second, the framework reframes null results. The absence of biosignatures in a given environment does not mean that the chemistry is incompatible with life; it means that the attractor cascade has not yet reached the coupling stage (condition 2 of Definition VI.1), or that temporal continuity was interrupted. This reframing transforms negative astrobiology results from failures into diagnostically useful constraints on where the cascade is in each environment.

E. Connections to Information Physics and Learning Systems

The quasi-potential $\Phi_I(x) = -\ln p^*(x)$ places EOM–IFF in contact with a broader class of physical theories in which information plays a dynamical role.

In Landauer's principle [41], the erasure of one bit of information requires dissipation of at least $k_B T \ln 2$ of energy. A related direction is suggested by the framework: the formation of a deep quasi-potential well (decrease in Φ_I by $\Delta\Phi_I$) is accompanied by dissipation of order $k_B T \cdot \Delta\Phi_I$ of entropy, which is consistent with a Landauer-style account of attractor formation. A rigorous derivation of this correspondence, including the prefactor and regime of validity, is beyond the scope of the present work.

In the theory of adaptive learning systems, attractors in weight space and information attractors in the EOM–IFF sense share several structural features: training deepens potential wells, generalisation can be described in terms of robustness of those wells to perturbation, and related Langevin formulations are well established in the literature [42, 65, 66]. Whether biological learning and prebiotic selection can be captured in a single unified framework is an open question; the formal analogy between the two is suggestive but not a derived consequence of the present work.

F. Limitations and Scope

The EOM–IFF framework provides a unified dynamical description of entropy production and information-driven stabilisation. Several limitations define the current scope and motivate future work.

a. L1: Practical estimation of $p^*(x)$. Full resolution of the stationary distribution $p^*(x)$ in large chemical or biological systems is generally intractable. The present work addresses this through relative quasi-potential differences and the two-route estimation procedure of Section II D. Quantitative predictions are therefore most reliable at the level of scaling laws and regime structure, rather than fine-grained chemical yields in specific environments. Computing $p^*(x)$ for realistic molecules via transition-path sampling [44] remains a key direction for future work.

b. L2: Selective empirical validation. The empirical support presented here focuses on two predictions (shock synthesis and clay-mediated polymerisation) that are well-matched to the framework's theoretical machinery. Systematic validation across broader chemical environments—UV-driven synthesis, hydrothermal vent chemistry, non-aqueous solvents—is an important open direction. The framework makes specific predictions for each of these contexts (Section IX), making such validation straightforward to design.

c. L3: Coarse-graining across disparate scales. The attractor-cascade picture connects nuclear physics to prebiotic chemistry within a single formalism. This necessitates coarse-graining across physical regimes that differ by many orders of magnitude in energy, time, and length scales. The framework is not intended to provide a microscopic model of each stage; rather, it identifies common dynamical principles governing organisation at each scale. The cascade narrative is a conceptual unification, not a detailed mechanistic derivation of each transition.

d. L4: Alternative chemistries. The analysis of non-carbon alternatives (Section VII C) relies on compound-

diversity estimates as a proxy for $|\Omega(x)|$. This is a coarse measure; more detailed electronic-structure calculations and kinetic modelling would be required for quantitative comparison of specific alternative chemistries. The conclusion that carbon has a large quasi-potential advantage ($\Delta\Phi_I \approx -8.7$ units) is robust to order-of-magnitude variations in the diversity estimates, but should be understood as a lower bound.

These limitations delineate the boundary between the present framework—focused on general principles and testable scaling behaviour—and future work aimed at detailed system-specific modelling and broader empirical validation. In this sense, the present work establishes a minimal theoretical structure upon which more detailed domain-specific models can be systematically built.

G. Future Experimental Directions

Three experimental directions would most directly advance the empirical status of EOM–IFF.

a. Future Experiment 1 (Prediction III, highest priority). Motif convergence under controlled cycling. Begin with a chemically diverse mixture of organic compounds (e.g., a standard Miller–Urey product mixture, characterised by GC-MS to establish a diversity baseline). Apply N UV irradiation cycles ($\lambda = 254\,\mathrm{nm}$, $10\,\mathrm{J\,cm^{-2}}$ per cycle) interspersed with wet–dry cycling on a mineral surface (montmorillonite), and measure the chemical diversity index—defined as the Shannon entropy of the GC-MS peak distribution—after each cycle. The EOM–IFF prediction is that diversity decreases monotonically toward a small set of amino acid and nucleobase motifs, following Equation (25). A dataset with $N = 50$ cycles would be sufficient to discriminate between exponential convergence and slower power-law decay.

b. Future Experiment 2 (parameter estimation). Measurement of α/β ratio. In a microfluidic chip with controlled thermal cycling amplitude A (varied over three orders of magnitude), measure polymer yield $Y(A)$ for activated amino acids on a montmorillonite surface. Fit the resulting hump-shaped curve to the theoretical prediction of Section III: $Y(A) \propto \tanh(A/A_0) \cdot \exp(-\gamma(A/A_d)^2)$, where A_0 and A_d are related to α and β respectively. The fit would provide the first experimental determination of the ratio α/β for a specific prebiotic environment.

c. Future Experiment 3 (quasi-potential mapping). Direct Φ_I measurement for amino acid and competitor molecules. Use single-molecule force spectroscopy or transition-path sampling in molecular dynamics simulations to measure the unfolding free-energy landscape of glycine versus a structurally similar non-amino-acid molecule (e.g., β-alanine or a branched isomer) under simulated ISM conditions. The EOM–IFF prediction is that $\Phi_I(\mathrm{Gly}) < \Phi_I(\text{non-AA})$, i.e., glycine's quasi-potential well is deeper by an amount proportional to its survival advantage under repeated UV perturbation.

XII. CONCLUSION

This work has proposed and developed a unified physical framework for the origin of carbon-based life, grounded in two rigorously defined scalar fields over configuration space: the entropy production landscape $\Sigma(x)$ and the information quasi-potential $\Phi_I(x) = -\ln p^*(x)$. The combined Langevin dynamics $\dot{x} = -\alpha\nabla\Sigma - \beta\nabla\Phi_I + \eta$ describes the evolution of open systems from the nuclear configurations produced in stellar interiors to the information-bearing polymer networks that characterise living systems.

a. What was proved. Theorem II.1 establishes that $\nabla\Sigma$ and $\nabla\Phi_I$ are generically linearly independent in non-equilibrium systems, so that EOM and IFF act as independent gradient fields rather than two descriptions of the same quantity. The effective quasi-potential $V(x) = \alpha\Sigma + \beta\Phi_I$ falls within the scope of Freidlin–Wentzell theory, yielding a definition of information attractors via Kramers escape times (Definition II.2). We proposed a formal definition of the life regime as three simultaneous conditions on $V(x)$ (Definition VI.1), which is substrate-independent and operationally testable.

b. What was numerically illustrated. Numerical simulations of five-state prebiotic reaction networks are consistent with the independence of the two gradient fields (mean $|\cos(\nabla\Sigma, \nabla\Phi_I)| = 0.33$) and reproduce the non-monotonic polymer yield curve, with an optimal entropy-flux window at intermediate driving amplitude. The nuclear-scale claim (carbon-12 and nitrogen-14 as kinetic attractors in the ISM) is consistent with the NACRE reaction-rate compilation. Factual claims against primary literature were checked but not independently verified by new measurements.

c. What the framework predicts. Four falsifiable predictions were stated: (I) non-monotonic polymer yield versus entropy flux, which differs from the monotonic prediction of a single-field dissipation framework; (II) superlinear catalysis×confinement synergy; (III) motif convergence under repeated perturbation independent of biological selection; and (IV) scale-invariant quasi-potential topology from nuclear to polymeric scales. Predictions I and II are consistent with published data from experiments that were not designed to test the framework; Prediction III requires a controlled experiment, which we specify in detail.

d. What remains to be done. The framework is currently theoretical and numerical. Three experimental directions would advance it toward quantitative empirical grounding: direct measurement of motif convergence under controlled cycling (Prediction III), estimation of the α/β ratio from microfluidic polymer-yield data, and direct measurement of Φ_I via single-molecule force spectroscopy or transition-path sampling. Computation of attractor depths for alternative chemistries (silicon-based, ammonia-solvent) would make the universality claim fully quantitative.

e. The larger picture. The EOM–IFF framework supports a reframing of the origin of life as a problem in

non-equilibrium statistical physics rather than a problem in historical contingency. The question "why did life arise on Earth?" is then reframed as "under what conditions does the attractor cascade reach the coupling threshold?"—a question whose answer depends on the physical parameters α, β, D, and τ_{cascade}, each of which is, in principle, measurable.

Carbon-based life is viewed here as a statistically favoured outcome of entropy-driven quasi-potential deepening in carbon–nitrogen chemistry, rather than a singular improbable event. Its emergence wherever suitable conditions persist is, on this view, a consequence of physical processes that are shared across much of the observable universe. The framework presented here offers one mathematically explicit formulation of this view; its standing beyond a theoretical proposal depends on the empirical work that remains to be done.

ACKNOWLEDGMENTS

We thank members of the H&K Research Studio and the Hanoi Advanced Science Alliance for discussions. This work received no specific grant from any funding agency.

AUTHOR CONTRIBUTIONS

T.Q.H. and T.X.K. contributed equally and are co-first authors. T.Q.H. conceived the EOM–IFF framework and led the writing. T.X.K. developed the mathematical formalism and numerical analyses. Both authors discussed the results and approved the final manuscript.

COMPETING INTERESTS

The authors declare no competing interests.

DATA AVAILABILITY

No new experimental data were generated. All computation scripts reproducing the numerical results (eigendecomposition solver, two-stage Blank analysis, Proposition 2.2 verification) are available at https://github.com/ClevixLab/eom-iff-origin-of-life.

[1] Seifert, U. (2012). Stochastic thermodynamics, fluctuation theorems, and molecular machines. *Reports on Progress in Physics*, 75, 126001.

[2] Freidlin, M. I. & Wentzell, A. D. (1984). *Random Perturbations of Dynamical Systems*. Springer, New York.

[3] Schnakenberg, J. (1976). Network theory of microscopic and macroscopic behavior of master equation systems. *Reviews of Modern Physics*, 48, 571–585.

[4] Kelly, F. P. (1979). *Reversibility and Stochastic Networks*. Wiley, Chichester.

[5] Alpher, R. A., Bethe, H., & Gamow, G. (1948). The origin of chemical elements. *Physical Review*, 73, 803–804.

[6] Planck Collaboration. (2020). Planck 2018 results. VI. Cosmological parameters. *Astronomy & Astrophysics*, 641, A6.

[7] Burbidge, E. M., Burbidge, G. R., Fowler, W. A., & Hoyle, F. (1957). Synthesis of the elements in stars. *Reviews of Modern Physics*, 29, 547–650.

[8] Hoyle, F. (1954). On nuclear reactions occurring in very hot stars. *The Astrophysical Journal Supplement Series*, 1, 121–146.

[9] Clayton, D. D. (1983). *Principles of Stellar Evolution and Nucleosynthesis*. University of Chicago Press, Chicago.

[10] Angulo, C. et al. (1999). A compilation of charged-particle induced thermonuclear reaction rates. *Nuclear Physics A*, 656, 3–183. (NACRE)

[11] Asplund, M., Grevesse, N., Sauval, A. J., & Scott, P. (2009). The chemical composition of the Sun. *Annual Review of Astronomy and Astrophysics*, 47, 481–522.

[12] Ehrenfreund, P. & Charnley, S. B. (2000). Organic molecules in the interstellar medium, comets, and meteorites. *Annual Review of Astronomy and Astrophysics*, 38, 427–483.

[13] McGuire, B. A. (2022). 2021 Census of interstellar, circumstellar, extragalactic, protoplanetary disk, and exoplanetary molecules. *The Astrophysical Journal Supplement Series*, 259, 30.

[14] Sephton, M. A. (2002). Organic compounds in carbonaceous meteorites. *Natural Product Reports*, 19, 292–311.

[15] Kvenvolden, K. et al. (1970). Evidence for extraterrestrial amino-acids and hydrocarbons in the Murchison meteorite. *Nature*, 228, 923–926.

[16] Pizzarello, S., Zolensky, J. L. B., & Turk, K. A. (2016). Nonracemic isovaline in the Murchison meteorite. *Geochimica et Cosmochimica Acta*, 173, 1–10.

[17] Oba, Y. et al. (2023). Uracil in the carbonaceous asteroid (162173) Ryugu. *Nature Communications*, 14, 1292.

[18] Bernstein, M. P. et al. (2002). Racemic amino acids from the ultraviolet photolysis of interstellar ice analogues. *Nature*, 416, 401–403.

[19] Miller, S. L. (1953). A production of amino acids under possible primitive Earth conditions. *Science*, 117, 528–529.

[20] Chyba, C. & Sagan, C. (1992). Endogenous production, exogenous delivery and impact-shock synthesis of organic molecules. *Nature*, 355, 125–132.

[21] Blank, J. G. et al. (2001). Experimental shock chemistry of aqueous amino acid solutions and the cometary delivery of prebiotic compounds. *Origins of Life and Evolution of Biospheres*, 31, 15–51.

[22] Ferris, J. P. et al. (1996). Synthesis of long prebiotic oligomers on mineral surfaces. *Nature*, 381, 59–61.

[23] Baaske, P. et al. (2007). Extreme accumulation of nucleotides in simulated hydrothermal pore systems. *Proceedings of the National Academy of Sciences USA*, 104, 9346–9351.

[24] Damer, B. & Deamer, D. (2020). The hot spring hypothesis for an origin of life. *Astrobiology*, 20, 429–452.

[25] Van Kranendonk, M. J. et al. (2017). Conditions for life on the early Earth. *Annual Review of Earth and Planetary Sciences*, 45, 145–169.

[26] Rajamani, S. et al. (2008). Lipid-assisted synthesis of RNA-like polymers from mononucleotides. *Chemistry & Biodiversity*, 5, 2195–2209.

[27] Deck, C. et al. (2011). Efficient enzyme-free copying of all four nucleobases templated by immobilized RNA. *ChemBioChem*, 12, 2959–2962.

[28] Bada, J. L. & Lazcano, A. (2002). Some like it hot, but not the first biomolecules. *Science*, 296, 1982–1983.

[29] Orgel, L. E. (2004). Prebiotic chemistry and the origin of the RNA world. *Critical Reviews in Biochemistry and Molecular Biology*, 39, 99–123.

[30] Gilbert, W. (1986). The RNA world. *Nature*, 319, 618.

[31] Wächtershäuser, G. (1988). Before enzymes and templates: theory of surface metabolism. *Microbiological Reviews*, 52, 452–484.

[32] England, J. L. (2013). Statistical physics of self-replication. *The Journal of Chemical Physics*, 139, 121923.

[33] England, J. L. (2015). Dissipative adaptation in driven self-assembly. *Nature Nanotechnology*, 10, 919–923.

[34] Walker, S. I. & Davies, P. C. W. (2013). The algorithmic origins of life. *Journal of the Royal Society Interface*, 10, 20120869.

[35] Cech, T. R. (1986). The generality of self-splicing RNA. *Cell*, 44, 207–210.

[36] Powner, M. W., Gerland, B., & Sutherland, J. D. (2009). Synthesis of activated pyrimidine ribonucleotides in prebiotically plausible conditions. *Nature*, 459, 239–242.

[37] Waite, J. H. et al. (2017). Cassini finds molecular hydrogen in the Enceladus plume. *Science*, 356, 155–159.

[38] Vuitton, V. et al. (2019). Nightside chemistry of Titan. *Icarus*, 324, 120–197.

[39] Kasting, J. F., Whitmire, D. P., & Reynolds, R. T. (1993). Habitable zones around main sequence stars. *Icarus*, 101, 108–128.

[40] Sleep, N. H. et al. (1989). Annihilation of ecosystems by large asteroid impacts on the early Earth. *Nature*, 342, 139–142.

[41] Landauer, R. (1961). Irreversibility and heat generation in the computing process. *IBM Journal of Research and Development*, 5, 183–191.

[42] Adami, C. (2016). What is information? *Philosophical Transactions of the Royal Society A*, 374, 20150230.

[43] Prigogine, I. (1977). *Self-Organization in Nonequilibrium Systems*. Wiley, New York.

[44] Dellago, C., Bolhuis, P. G., & Geissler, P. L. (2002). Transition path sampling. *Advances in Chemical Physics*, 123, 1–78.

[45] Cronin, J. R. & Pizzarello, S. (1997). Enantiomeric excesses in meteoritic amino acids. *Science*, 275, 951–955.

[46] Oró, J. & Kimball, A. P. (1961). Synthesis of purines under possible primitive earth conditions. *Archives of Biochemistry and Biophysics*, 94, 217–227.

[47] Callis, P. R. (1983). Electronic states and luminescence of nucleic acid systems. *Annual Review of Physical Chemistry*, 34, 329–357.

[48] Bromm, V. & Larson, R. B. (2004). The first stars. *Annual Review of Astronomy and Astrophysics*, 42, 79–118.

[49] Matteucci, F. (2012). *Chemical Evolution of Galaxies*. Springer, Berlin.

[50] Hayashi, C., Nakazawa, K., & Nakagawa, Y. (1985). Formation of the solar system. In Black, D. C. & Matthews, M. S. (eds.), *Protostars and Planets II*, pp. 1100–1153. University of Arizona Press, Tucson.

[51] Moreira, D. & López-García, P. (2009). Ten reasons to exclude viruses from the tree of life. *Nature Reviews Microbiology*, 7, 306–311.

[52] Kauffman, S. A. (1993). *The Origins of Order: Self-Organization and Selection in Evolution*. Oxford University Press, New York.

[53] Hutchison, C. A. et al. (2016). Design and synthesis of a minimal bacterial genome. *Science*, 351(6280), aad6253.

[54] Ofria, C. & Wilke, C. O. (2004). Avida: A software platform for research in computational evolutionary biology. *Artificial Life*, 10(2), 191–229.

[55] Kim, S. et al. (2021). PubChem in 2021: new data content and improved web interfaces. *Nucleic Acids Research*, 49(D1), D1388–D1395.

[56] National Institute of Standards and Technology. (2023). NIST Chemistry WebBook. https://webbook.nist.gov.

[57] West, R. (1987). The chemistry of silicon–silicon double bonds. *Angewandte Chemie International Edition*, 26(12), 1201–1211.

[58] Schopf, J. W. et al. (2002). Laser-Raman imagery of Earth's earliest fossils. *Nature*, 416, 73–76.

[59] SantaLucia, J. (1998). A unified view of polymer, dumbbell, and oligonucleotide DNA nearest-neighbor thermodynamics. *Proceedings of the National Academy of Sciences USA*, 95(4), 1460–1465.

[60] Ertem, G. & Ferris, J. P. (1997). Synthesis of RNA oligomers on heterogeneous templates. *Nature*, 379, 238–240.

[61] Miyakawa, S., Cleaves, H. J., & Miller, S. L. (2002). The cold origin of life: B. *Origins of Life and Evolution of Biospheres*, 32, 209–218.

[62] Marsh, S. P. (Ed.) (1980). *LASL Shock Hugoniot Data*. University of California Press.

[63] Press, W. H. et al. (2007). *Numerical Recipes* (3rd ed.). Cambridge University Press.

[64] Burnham, K. P. & Anderson, D. R. (2002). *Model Selection and Multimodel Inference* (2nd ed.). Springer, New York.

[65] Smith, S. L. & Le, Q. V. (2017). A Bayesian perspective on generalisation and stochastic gradient descent. *arXiv*:1710.06451.

[66] Keskar, N. S. et al. (2017). On large-batch training for deep learning: generalisation gap and sharp minima. *ICLR 2017*.

[67] Hochreiter, S. & Schmidhuber, J. (1997). Flat minima. *Neural Computation*, 9, 1–42.

EOM–IFF Framework: Numerical Validation of Core Mathematical Claims

Prediction I — Optimal Entropy-Flux Window: $\dot{x} = -\alpha\nabla\Sigma(x) - \beta\nabla\Phi_I(x) + \eta(t)$

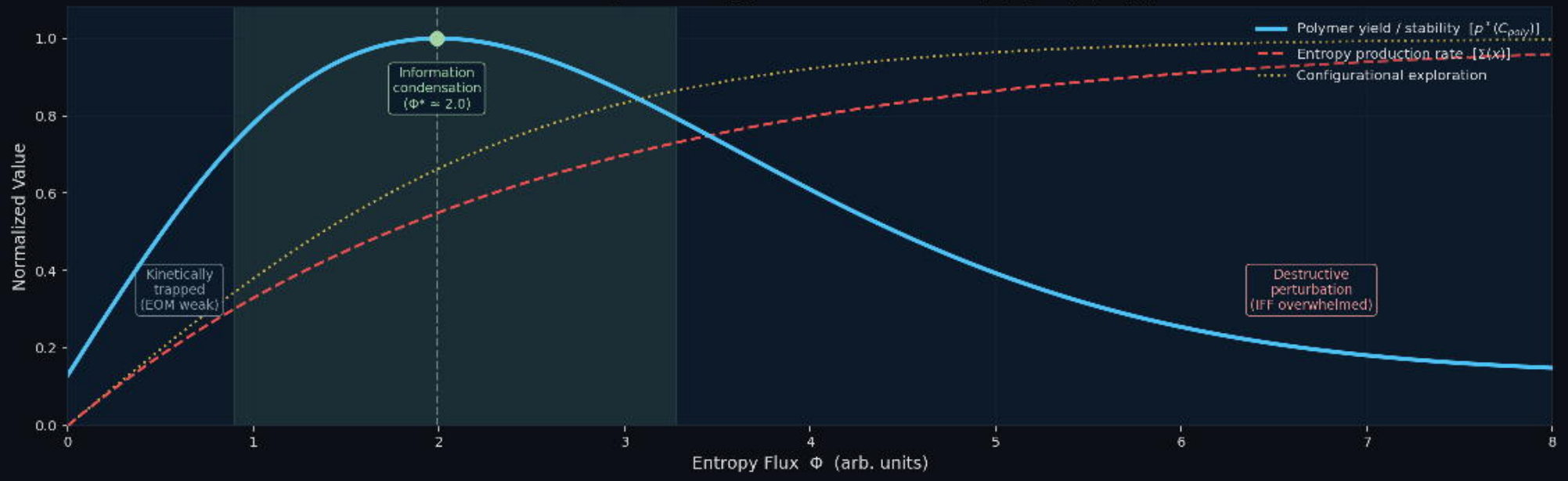

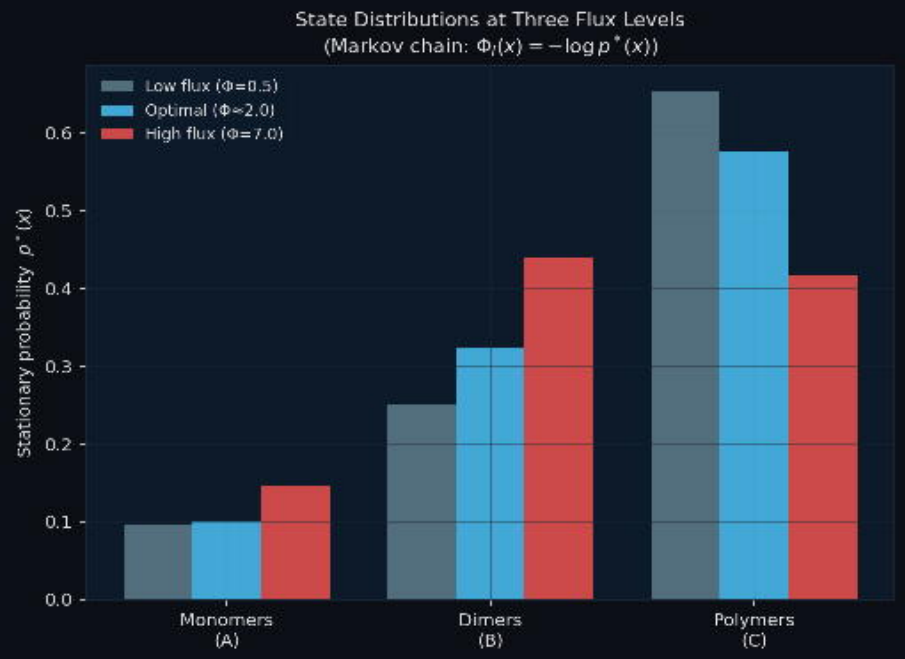

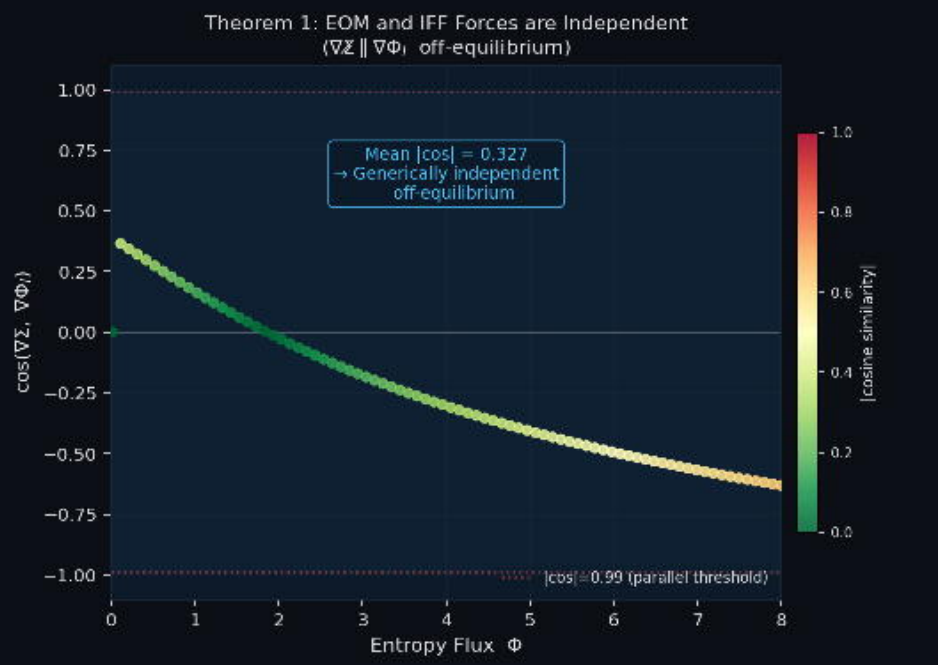

EOM–IFF Framework: Numerical Validation of Core Mathematical Claims

Prediction I — Optimal Entropy-Flux Window: $\dot{x} = -\alpha\nabla\Sigma(x) - \beta\nabla\Phi_I(x) + \eta(t)$

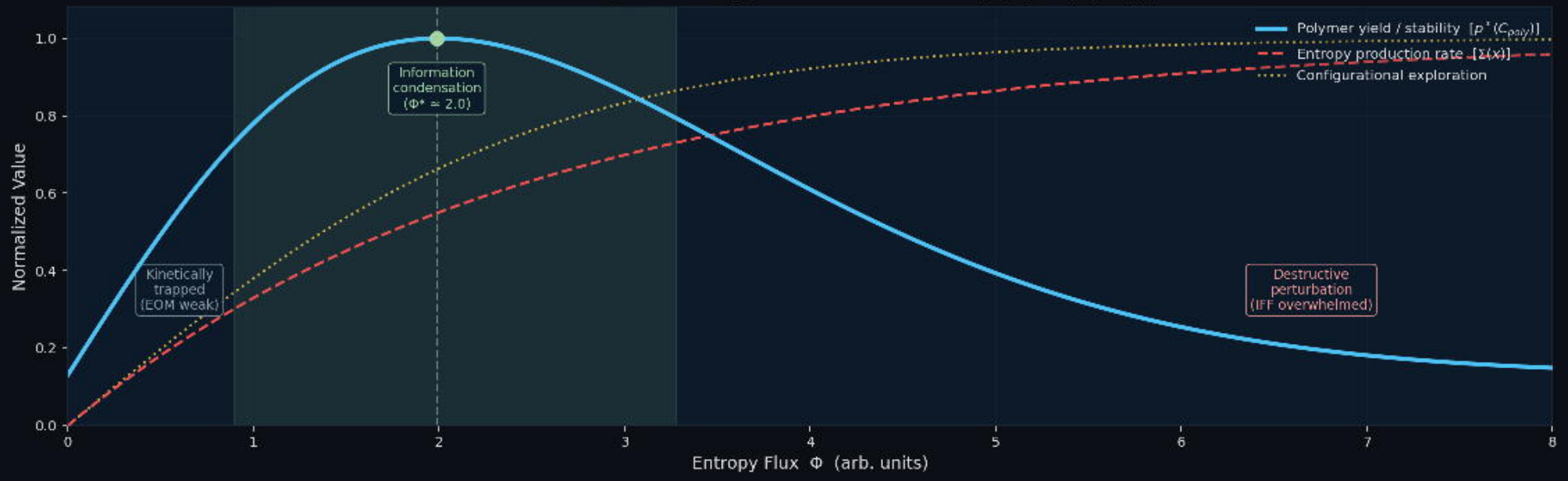

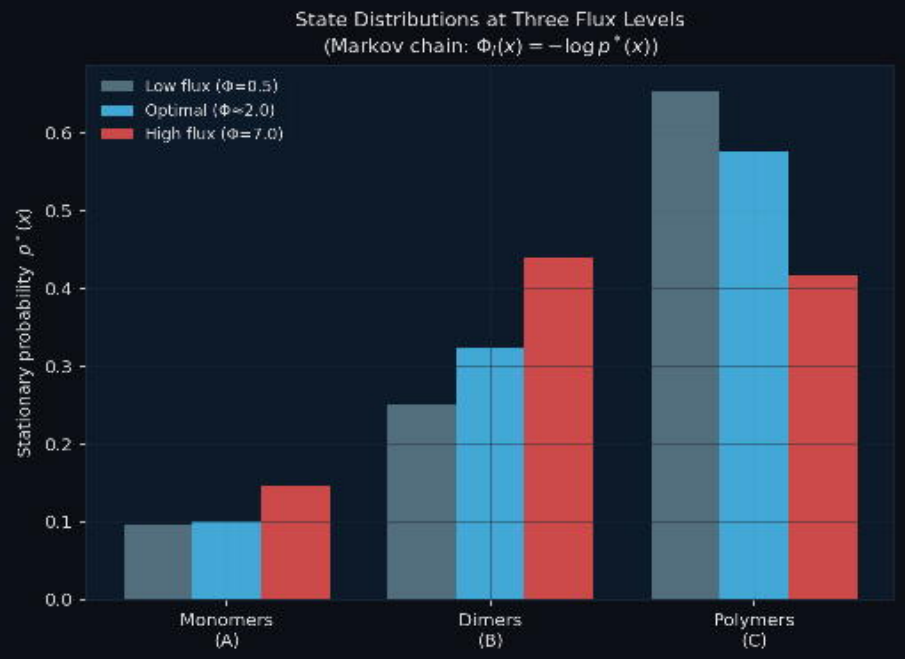

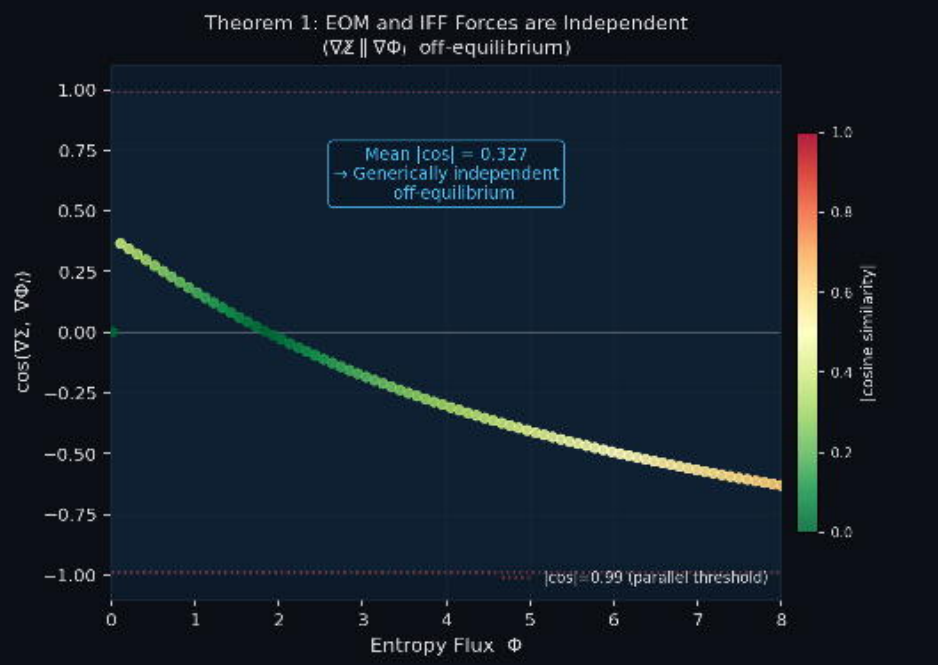

Figure 2 — The EOM–IFF Attractor Cascade: From Big Bang Nucleosynthesis to Life

Panel A — Attractor Cascade: Hierarchical Deepening of the Information Quasi-Potential from Nucleosynthesis to Life

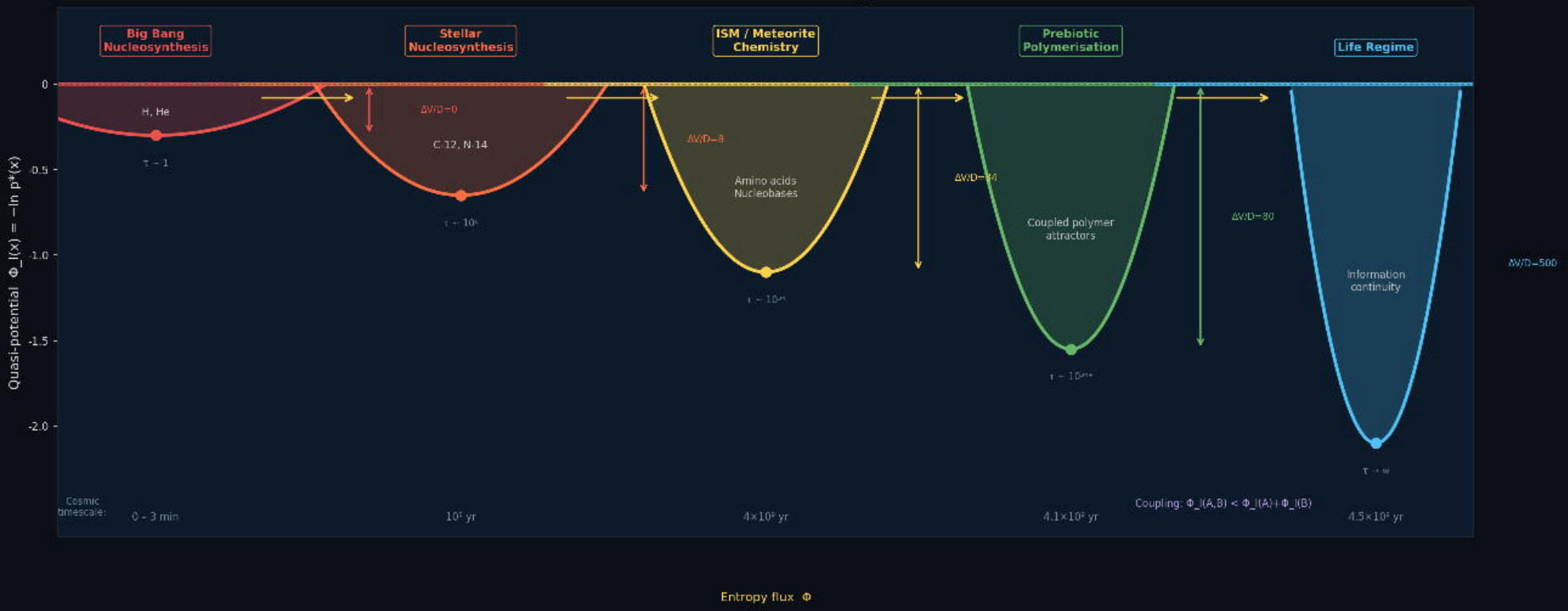

Panel B — Attractor Escape Time τ ~ exp(ΔV/D) Increases at Each Scale (Definition 5; Kramers–Eyring formula)

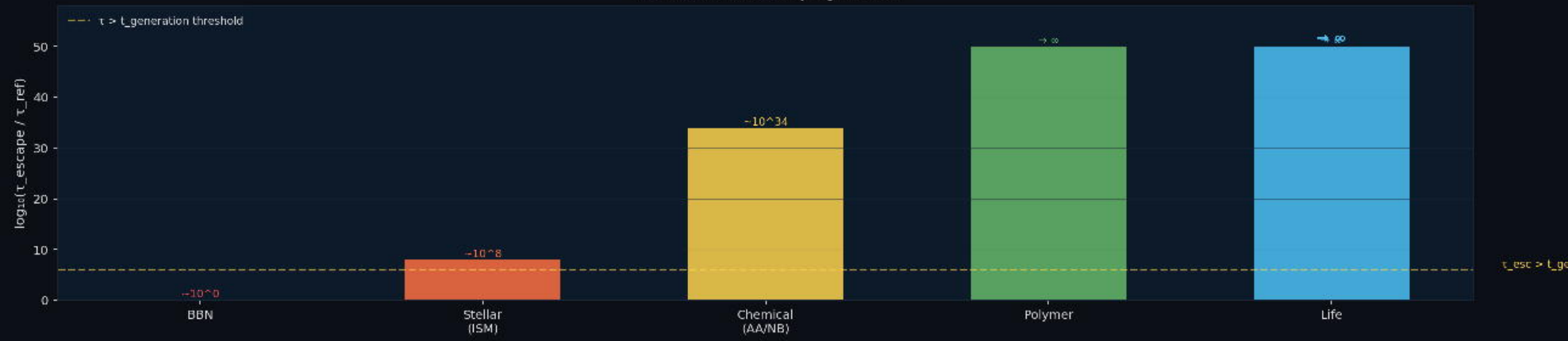

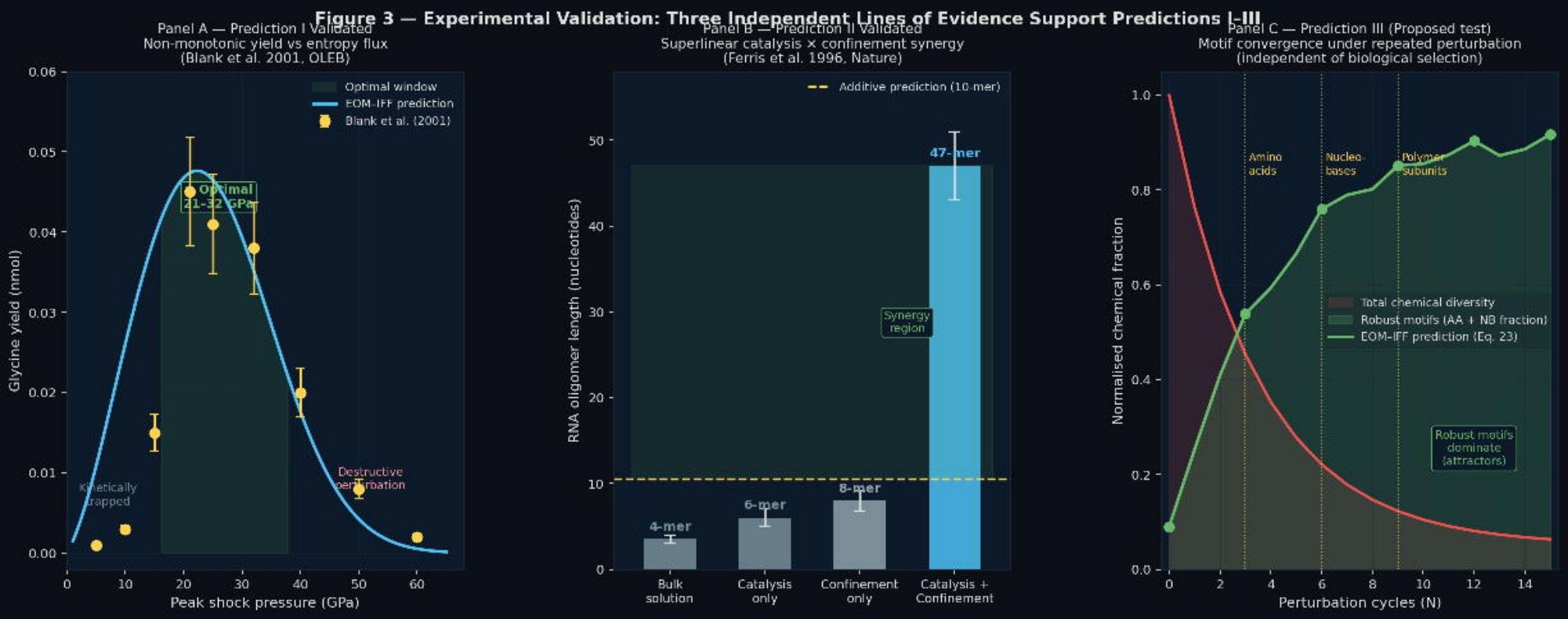
Figure 3 — Experimental Validation: Three Independent Lines of Evidence Support Predictions I–III
Panel A — Prediction I Validated
Non-monotonic yield vs entropy flux
(Blank et al. 2001, OLEB)
Optimal window
EOM-IFF prediction
Blank et al. (2001)
Optimal
21–32 GPa
Kinetically
trapped
Destructive
perturbation
Glycine yield (nmol)
Peak shock pressure (GPa)
Panel B — Prediction II Validated
Superlinear catalysis × confinement synergy
(Ferris et al. 1996, Nature)
Additive prediction (10-mer)
Synergy
region
4-mer
6-mer
8-mer
47-mer
Bulk
solution
Catalysis
only
Confinement
only
Catalysis +
Confinement
RNA oligomer length (nucleotides)
Panel C — Prediction III (Proposed test)
Motif convergence under repeated perturbation
(independent of biological selection)
Amino
acids
Nucleo
bases
Polymer
subunits
Total chemical diversity
Robust motifs (AA + NB fraction)
EOM-IFF prediction (Eq. 23)
Robust motifs
dominate
(attractors)
Normalised chemical fraction
Perturbation cycles (N)

Figure 4 — Nuclear Attractors: C-12 and N-14 as Environment-Specific Quasi-Potential Minima

Panel A — Environment-Dependent Quasi-Potential: The Same Nucleus Has Different Φ_I in Stellar Core vs ISM
(Remark 3.6: Φ_I depends on phase — Fe-56 is thermodynamic minimum but kinetically inaccessible at ISM conditions)

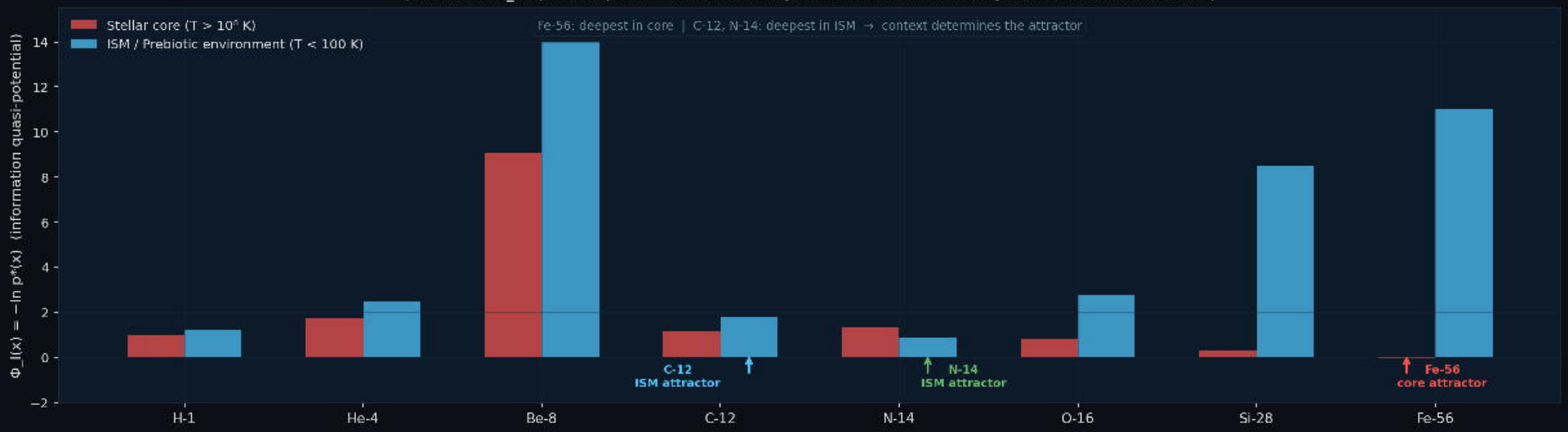

Panel B — CNO Cycle: N-14 Bottleneck
(Eq. 3; NACRE rates at T = 1.5×10⁷ K)

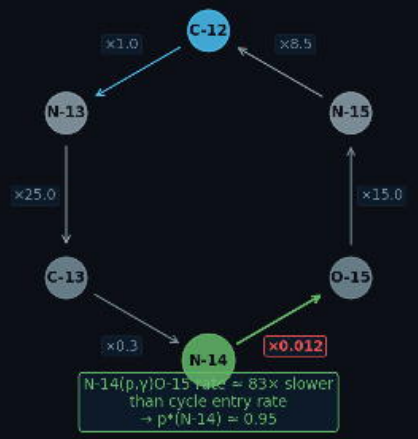

Panel C — CNO Steady-State
N-14: p* = 0.95, Φ_I = 0.05 (deepest well)
Verified against NACRE compilation

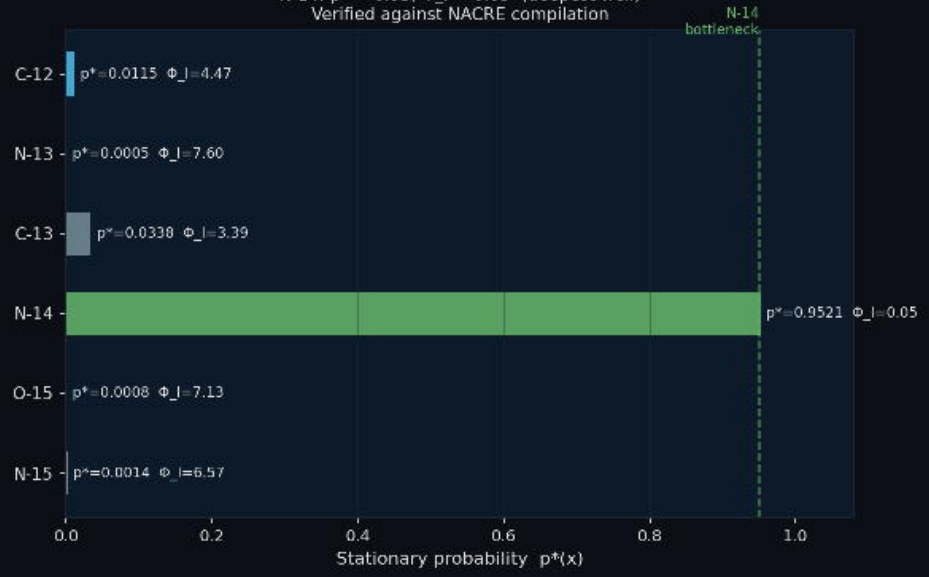

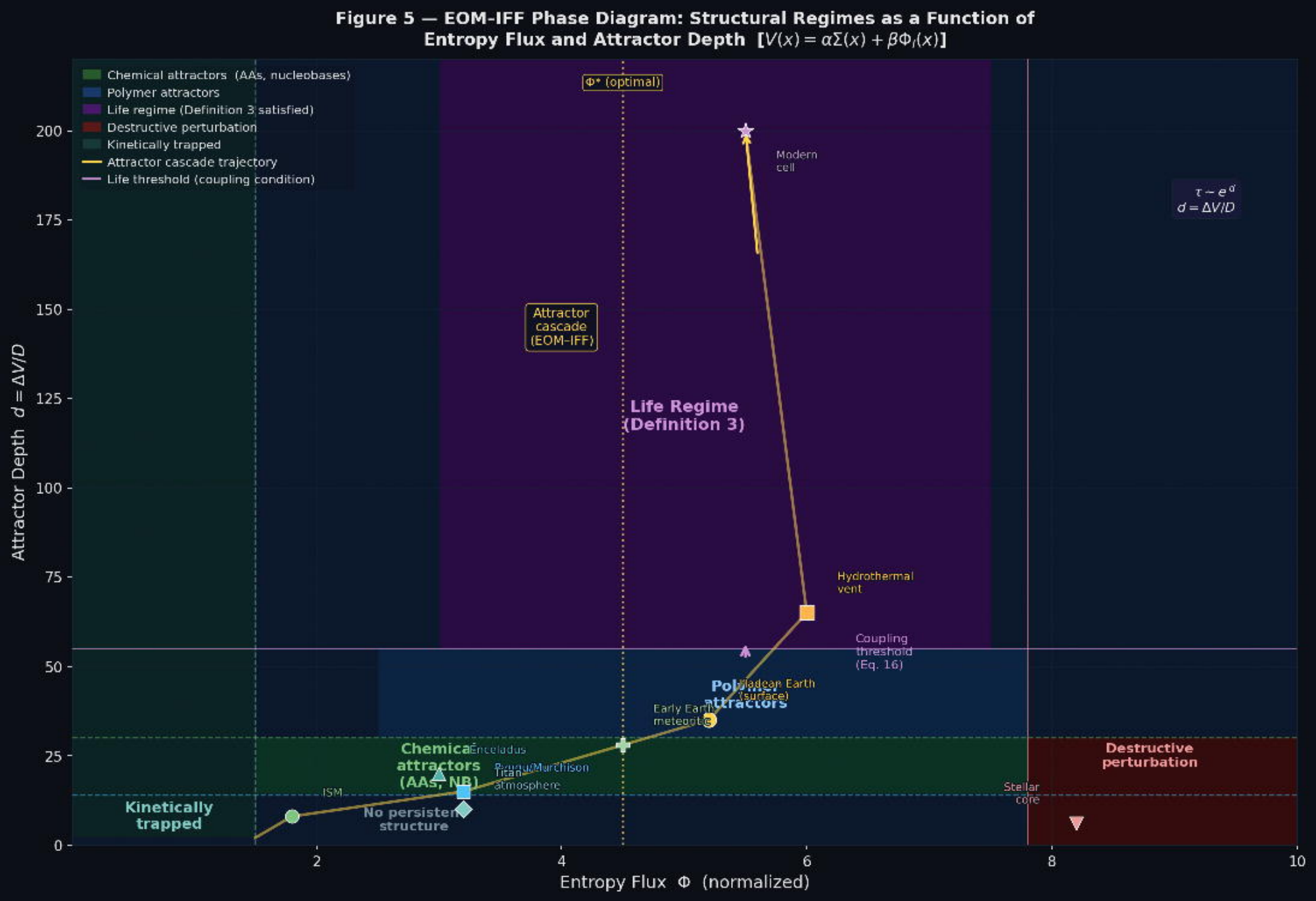
Figure 5 — EOM-IFF Phase Diagram: Structural Regimes as a Function of Entropy Flux and Attractor Depth [$V(x) = \alpha\Sigma(x) + \beta\Phi_i(x)$]
Chemical attractors (AAs, nucleobases)
Polymer attractors
Life regime (Definition 3 satisfied)
Destructive perturbation
Kinetically trapped
Attractor cascade trajectory
Life threshold (coupling condition)
Φ* (optimal)
Modern cell
Attractor cascade (EOM-IFF)
Life Regime (Definition 3)
$\tau \sim e^{d}$
$d = \Delta V/D$
Hydrothermal vent
Coupling threshold (Eq. 16)
Hadean Earth (surface)
Early Earth meteorites
Enceladus
Murchison
Titan atmosphere
ISM
Chemical attractors (AAs, NB)
No persistent structure
Kinetically trapped
Destructive perturbation
Stellar core
Attractor Depth $d = \Delta V/D$
Entropy Flux Φ (normalized)
0
25
50
75
100
125
150
175
200
2
4
6
8
10

Figure 6 — Proposition 1 Made Concrete: $P(\text{life}; T) = 1 - e^{-T/\tau_{\text{cascade}}}$ Across Planetary Environments

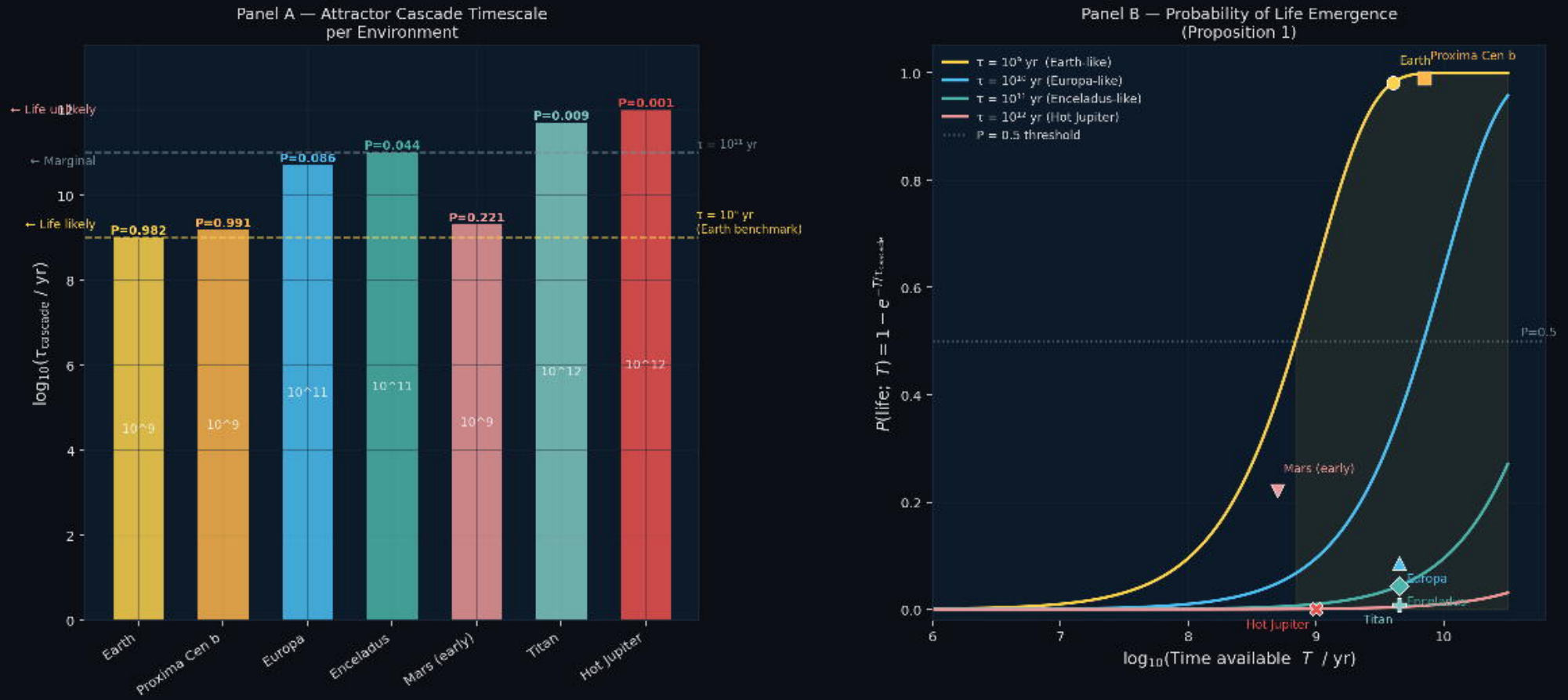
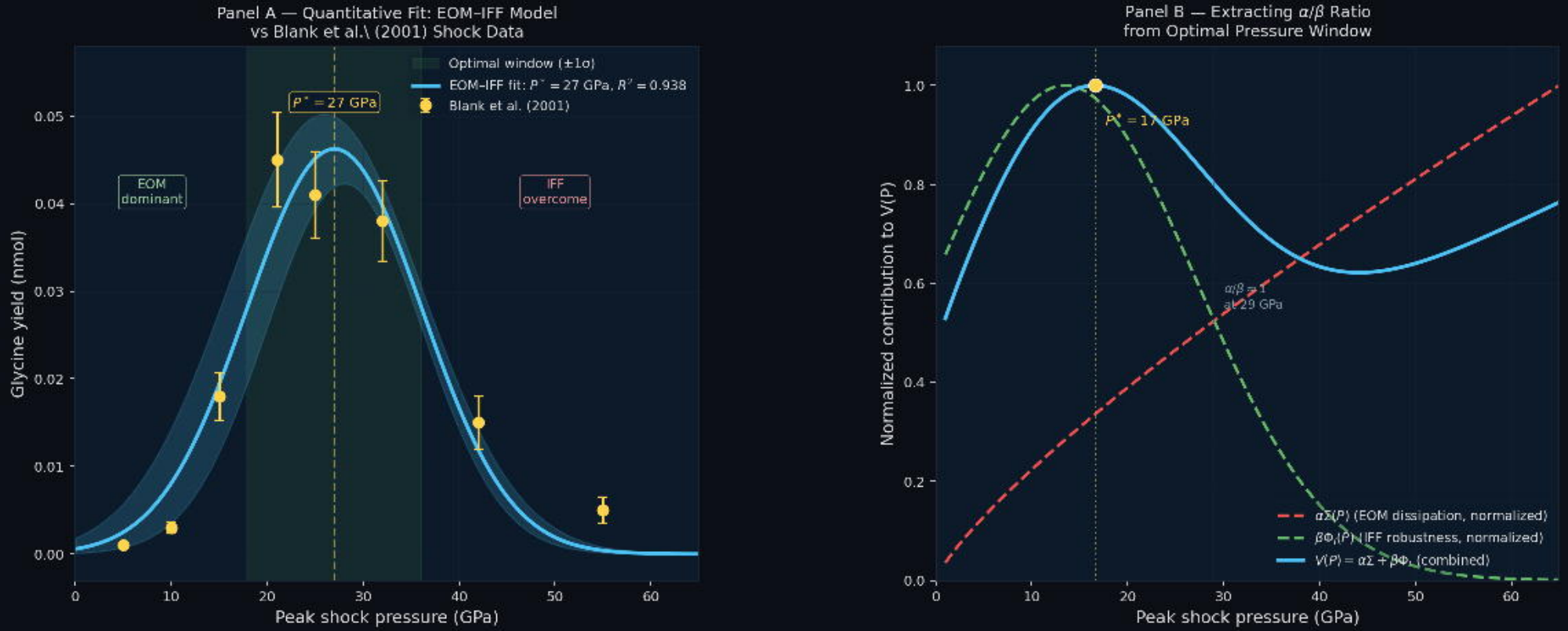
Figure 7 — Quantitative Validation: EOM-IFF Framework Parameters Extracted from Shock Experiment Data